Molecular Shuttling in Rotaxanes: Control over Proximity and Charge Recombination

Maximilian Wolf, Ayumu Ogawa, Mareike Bechtold, Maxime Vonesch, Jennifer A. Wytko, Koji Oohora, Stéphane Campidelli, Takashi Hayashi, Dirk M. Guldi and Jean Weiss

email: dirk.guldi@fau.de, jweiss@unistra.fr and thayashi@chem.eng.osaka-u.ac.jp

SUPPORTING INFORMATION

Experimental Section

For the transient absorption spectroscopy within the time window of 0 to 6000 ps an Ultrafast Systems Helios pump/probe transient absorption spectrometer was used. An Ultrafast Systems Eos spectrometer with a built-in supercontinuum laser source was utilized for delays from 1 ns to 400 µs. The excitation was performed with Clark-MXR Ti:Sapphire CPA2101 and CPA2110 laser systems with a pulse width of ~150 fs. The samples were measured in 2 mm glass cuvettes and excited at the 420-430 nm Soret band of the porphyrin. Samples were measured in Tol (Roth Rotisol for HPLC), PhCl (Acros Organics 99.9 for HPLC) and PhCN (Sigma Aldrich 99.9 for HPLC) at concentrations of $5x10^{-5}$ M. To investigate coordination processes, the samples were measured in a solution of 10^{-3} M pyridine in Tol and CB.

For absorption measurements, a Perkin Elmer Lambda 2 spectrometer was used. All measurements were performed in 10x10 mm quartz glass cuvettes with a transmission window of 200-2500 nm. For fluorescence spectroscopy, a Horiba Jobin Yvon Lambda FluoroMax-3 spectrometer was used. The measurements were performed with an integration time of 0.5 seconds and entrance and exit slits set to 2 nm. The same cuvettes as for absorption spectroscopy were used.

General Synthetic Methods. All reagents were purchased from commercial sources and used without further purification unless otherwise stated, THF was distilled over Na/benzophenone under argon. Saturated $EDTA_{aq}$ and 1 M $NaOH_{aq}$ were prepared before the experiment. The 0.10 M solution of base in THF was prepared under argon before the experiment. ^{1}H NMR spectra were collected on a Bruker Avance Ⅲ (500 MHz) spectrometer. The chemical shifts are reported in ppm relative to a residual solvent peak. ESI-TOF MS analyses were performed with a Bruker Daltonics microTOF II mass spectrometer.

Synthesis of free base rotaxane 1. $Cu(MeCN)_4PF_6$ (12 mg, 33 µmol, 0.96 eq) was added to a degassed solution of zinc(II) strapped-porphyrin **4Zn** (29 mg, 34 µmol) in dry THF (3.4 mL) and the solution was stirred under argon at r.t. for 30 min. The azide **2** (24 mg, 41 µmol, 1.2 eq), alkyne **3** (30 mg, 34 µmol, 1.0 eq) and di-*iso*-propylethylamine (0.10 M in THF, 0.34 mL, 34 µmol, 1.0 eq) were added and the solution was stirred at 65 °C for 22 h. The solution was cooled to r.t., diluted with CH_2Cl_2 (20 mL) and washed with saturated $EDTA_{aq}$. The organic layer was dried over $NaSO_4$ and evaporated to dryness. The solid was dissolved in CH_2Cl_2 (20 mL) and treated with trifluoroacetic acid (2 mL) at r.t. for 4 h. The green solution was washed with 1 M $NaOH_{aq}$ and then with saturated $NaCl_{aq}$, dried over Na_2SO_4 and filtered. After removal of the solvents under reduced pressure, the product was purified by two column chromatographies (both columns SiO_2, CH_2Cl_2/MeOH (50/1); the second column was a water-jacketed column) to afford the freebase rotaxane **1** (37 mg, 16 µmol, 48%). ^{1}H NMR ($CDCl_3$, 500 Hz) δ ppm: 9.34 (s, 1H), 8.97 (d, J = 4.5

Hz, 2H), 8.94 (s, 1H), 8.73 (m, 2H), 8.66 (m, 6H),8.02 (s, 2H), 7.93 (m, 2H), 7.84 (m, 4H), 7.78 (d, J = 7.7 Hz, 2H), 7.67 (d, J = 8.0 Hz, 2H), 7.41 (s, 2H), 7.38 (td, J = 9.2 Hz, J = 2.8 Hz, 12H), 7.32 (dd, J = 8.2 Hz, J = 1.7 Hz, 2H), 7.05 (m, 4H), 6.77 (d, J = 8.6 Hz, 2H), 6.72 (d, J = 8.2 Hz, 2H), 6.69 (d, J = 8.2 Hz, 2H), 5.09 (s, 1H), 5.07 (d, J = 15.0 Hz, 1H), 4.35 (d, J = 8.6 Hz, 2H), 4.30 (d, J = 15.0 Hz, 1H), 4.13 (s, 1H), 2.98 (s, 3H), 1.35 (s, 27H), 0.48 (m, 2H), -1.16 (m, 2H), -3.18 (s, 2H), -3.84 (m, 2H). ^{13}C NMR ($CDCl_3$, 125 Hz) δ ppm: 158.50, 158.47, 156.3, 154.41, 154.03, 153.69, 153.48, 148.1, 147.3, 146.91, 146.53, 146.37, 146.27, 146.25, 146.20, 146.14, 146.13, 146.01, 145.94, 145.59, 145.53, 145.42, 145.34, 145.30, 145.22, 145.17, 145.02, 144.81, 144.74, 144.52, 144.43, 143.23, 143.02, 142.73, 142.60, 142.57, 142.51, 142.36, 142.28, 142.25, 142.18, 142.14, 142.09, 142.01, 141.98, 141.80, 141.73, 141.71, 140.22, 140.19, 139.94, 139.69, 139.51, 139.02, 139.00, 138.04, 136.83, 136.63, 135.97, 135.86, 135.11, 133.06, 133.00, 132.72, 132.02, 130.73, 130.59, 130.46, 130.02, 129.90, 129.87, 129.80, 129.12, 128.68, 128.38, 127.5, 125.99, 125.81, 125.79, 124.4, 122.3, 117.5, 116.6, 111.9, 106.1, 104.9, 83.5, 70.2, 69.1, 63.4, 60.3, 50.9, 43.1, 40.3, 34.4, 31.5, 23.1, 1.1. UV-Visible (chlorobenzene) λ / nm (ε / $M^{-1}cm^{-1}$): 418.5 (3.1 x 10^5), 509 (1.8 x 10^4), 543 (5.9 x 10^3), 583 (6.5 x 10^3), 636 (2.2 x 10^3). ESI-TOF MS: calc. m/z $[C_{167}H_{94}N_{10}O]+H^+$: 2256.77; found: 2256.76.

Synthesis of zinc(II) rotaxane 1Zn. A solution of rotaxane **1** (20 mg, 8.9 μmol) and $Zn(OAc)_2•2H_2O$ (19 mg, 89 μmol) in THF (2.3 mL) was heated at 60 °C for 17 h. The solution was cooled to r.t and evaporated to dryness. Purification by column chromatography over silica gel (CH_2Cl_2/MeOH (50/1)), followed by precipitation from CH_2Cl_2/MeOH gave the zinc rotaxane **1Zn** (16 mg, 7 μmol) in 78% yield. ^{1}H NMR ($CDCl_3$, 500 Hz) δ ppm: 10.30 (s, 1H), 9.72 (s, 1H), 9.45 (d, J = 4.3 Hz, 1H), 9.44 (d, J = 4.3 Hz, 1H), 9.30 (br s, 1H), 9.10 (d, J = 4.6 Hz, 1H), 9.09 (d, J = 4.6 Hz, 1H), 8.95 (d, J = 4.3 Hz, 2H), 8.78 (m, 2H), 8.68 (d, J = 4.3 Hz, 1H), 8.67 (d, J = 4.3 Hz, 1H), 7.84 (d, J = 8.2 Hz, 2H), 7.78 (m, 4H), 7.50 (m, 2H), 7.46 (s, 2H), 7.22 (s, 10H), 7.02 (d, J = 8.5 Hz, 6H), 6.62 (d, J = 8.7 Hz, 2H), 6.39 (d, J = 8.0 Hz, 2H), 6.23 (m, 4H), 5.93 (t, J = 9.1 Hz, 4H), 5.46 (d, J = 6.5 Hz, 2H), 4.75 (d, J = 9.1 Hz, 1H), 4.55 (s, 1H), 4.00 (d, J = 9.1 Hz, 1H), 2.52 (s, 3H), 2.22 (s, 2H), 1.31 (s, 27H), -0.70 (br m, 1H), -0.90 (br m, 1H), -2.04 (br m, 1H), -2.19 (br m, 1H). ^{13}C NMR ($CDCl_3$, 125 Hz) δ ppm: 159.3, 156.2, 155.8, 153.93, 153.29, 153.12,150.49, 150.43, 150.29, 150.24, 148.72, 148.33, 148.02, 147.3, 146.55, 146.39, 146.25, 146.15, 146.10, 146.05, 145.94, 145.88, 145.69, 146.64, 145.47, 145.44, 145.39, 145.35, 145.26, 145.23, 145.22, 145.16, 145.10, 144.96, 144.65, 144.49, 144.33, 144.27, 143.0, 142.88, 142.67, 142.65, 142.61, 142.50, 142.47, 142.37, 142.14, 142.03, 141.97, 141.93, 141.61, 141.22, 141.03, 140.96, 140.06, 140.00, 139.58, 139.49, 138.5, 137.7, 136.46, 136.42, 136.38, 136.05, 135.98, 135.64, 135.27, 132.89, 132.18, 131.89, 131.41, 131.13, 130.72, 130.63, 130.18, 130.17, 128.6, 127.91, 127.57, 127.08, 126.11, 126.04, 125.37, 124.08, 122.79, 122.69, 116.72, 116.70, 112.3, 106.8, 104.8, 83.21, 69.8, 68.9, 64.1, 63.0, 53.5, 41.8, 39.9, 34.4, 31.5, 29.8, 24.1. UV-Visible (chlorobenzene) λ / nm (ε / $M^{-1}cm^{-1}$): 427.5 (3.9 x 10^5), 557 (2 x 10^4), 595 (4 x 10^3). ESI-TOF MS: calc. m/z

$[C_{167}H_{92}N_{10}OZn]+H^+$ 2319.69; found: 2319.67; calc. m/z $[C_{167}H_{92}N_{10}OZn]+2H^+$: 1160.35; found: 1160.35.

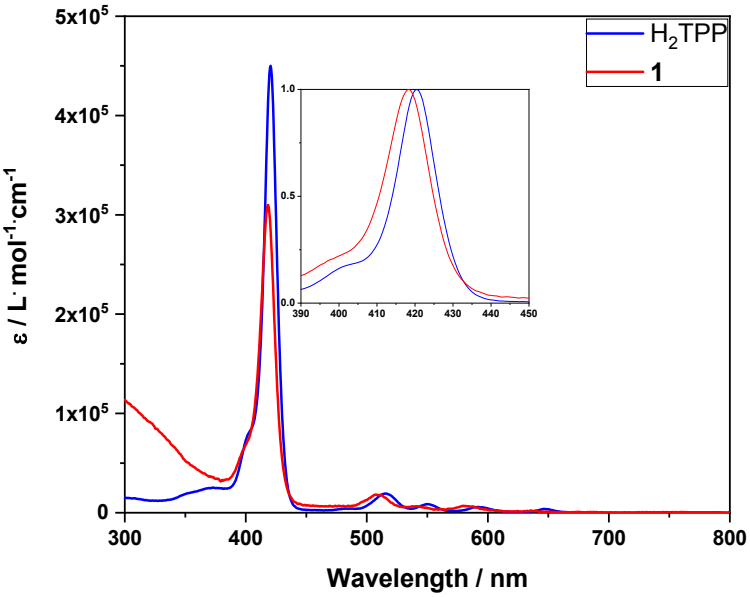

Figure S1: Steady-state absorption spectrum of **1** in comparison to H_2TPP. Inset: normalized Soret absorption bands, highlighting the absorption shift.

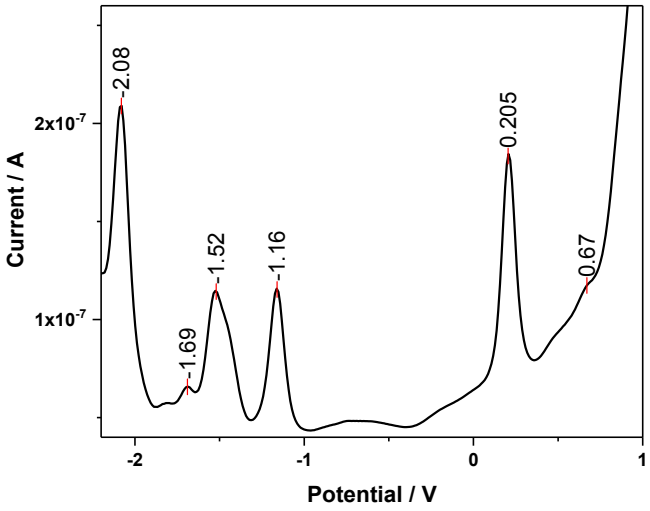

Figure S2: Squarewave votammogram of **1Zn** measured from -2.2 to 1 V vs. $Ag/AgNO_3$ with a glassy carbon working electrode and a Pt counter electrode. The solvent was o-DCB with 0.1 M $TBAClO_4$ as supporting electrolyte.

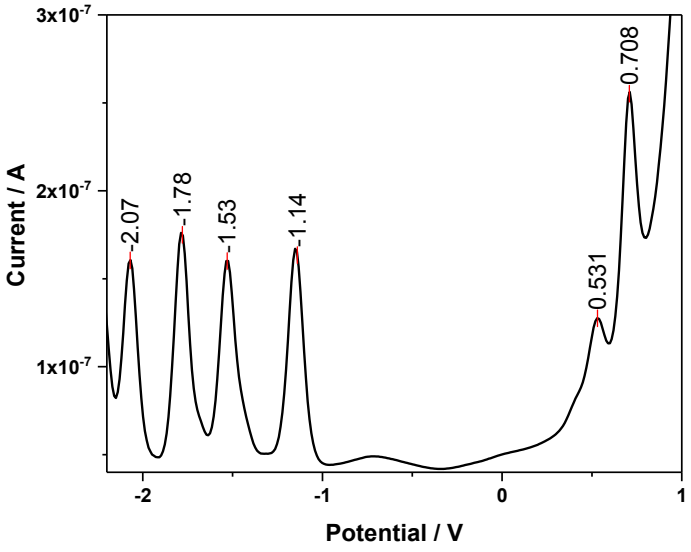

Figure S3: Squarewave voltammogram of **1** measured from -2.2 to 1.5 V vs. $Ag/AgNO_3$ on a glassy carbon working electrode and a Pt counter electrode. The solvent was o-DCB with 0.1 M $TBAClO_4$ as supporting electrolyte.

Table S1: Summary of quantum yields by using H_2TPP as reference in various solvents.

Solvent	Φ_{fl} of **1** in %
Tol	0.70
PhCl	$5.1x10^{-3}$
PhCN	0.03

Table S2: Calculated driving forces for charge separation and charge recombination of **1** – the dielectric constants were taken from reference 1

Solvent	ε_S	ΔG_{CS} in eV	ΔG_{CR} (GS) in eV	ΔG_{CR} ($^{3*}C_{60}$) in eV	ΔG_{CR} ($^{3*}H_2P$) in eV
Tol	2.38	0.28a	-2.22[a]	-0.72	-0.8
PhCl	5.62	-0.23	-1.71	-0.21	-0.29
PhCN	25.2	-0.52	-1.42	0.08	0.00

[a] the dielectric continuum model employed in calculating these values overestimates the influence of low polarity solvents

Common for H_2P-C_{60} conjugates, driving forces of charge separation are significantly smaller in **1** compared to **1Zn**. In turn, energies of the formed CSS are higher. Although the dielectric continuum model is poorly adapted to very apolar solvents such as toluene, it is apparent that CS and CR are strongly influenced by solvent polarity. Due to the low-energy triplet excited states, CR proceeds to a great extent via population of either $^3C_{60}$ or ^3H_2P, which decreases with increasing solvent polarity, as the energy gap between CSS and triplet excited states diminishes.

[1] A. A. Maryott, E. R. Smith, *National Bureau of Standards Gaithersburg MD* **1951**.

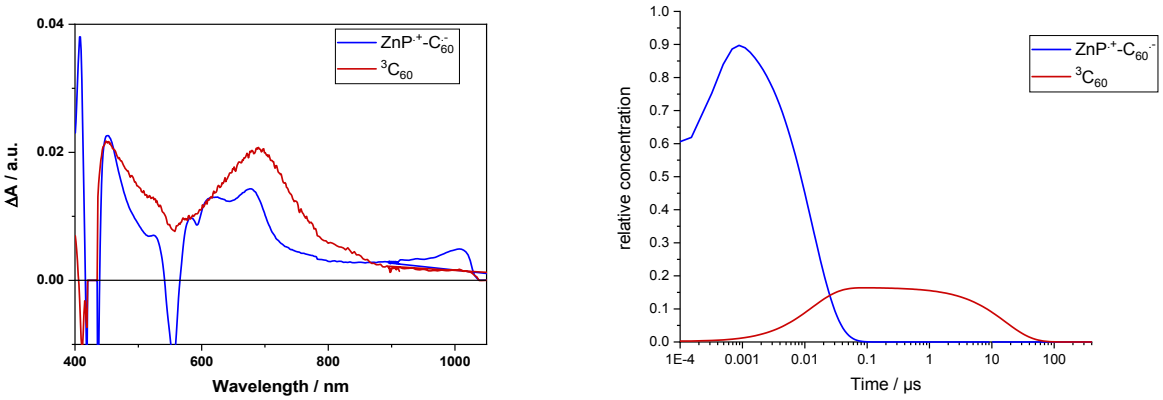

Figure S4: Deconvoluted species associated spectra (SAS) and corresponding concentration profiles of **1Zn** in toluene depicting the CSS (denoted as $ZnP^{\cdot+}$-$C_{60}^{\cdot-}$) and triplet excited state (denoted as $^{3*}C_{60}$) obtained from target analysis.

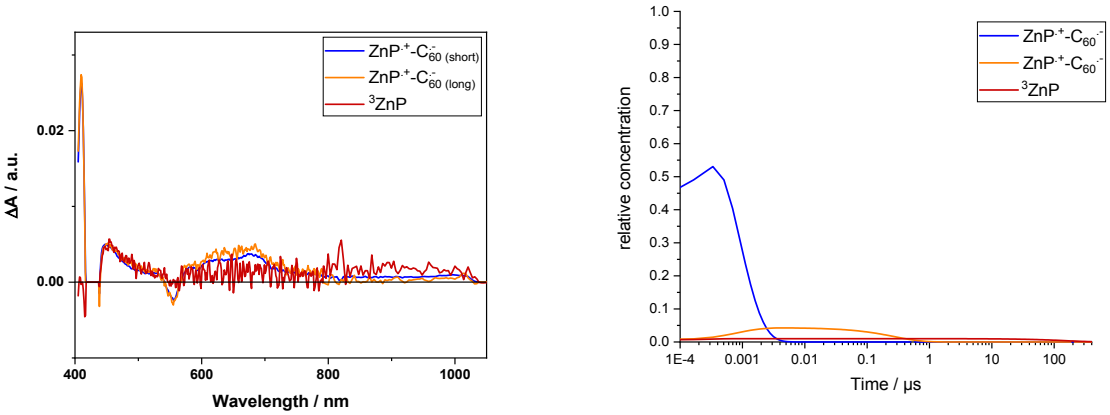

Figure S5: Deconvoluted species associated spectra (SAS) and corresponding concentration profiles of **1Zn** in benzonitrile depicting two CSS with different lifetime (denoted as $ZnP^{\cdot+}$-$C_{60}^{\cdot-}$) and triplet excited state (denoted as ^{3*}ZnP) obtained from target analysis.

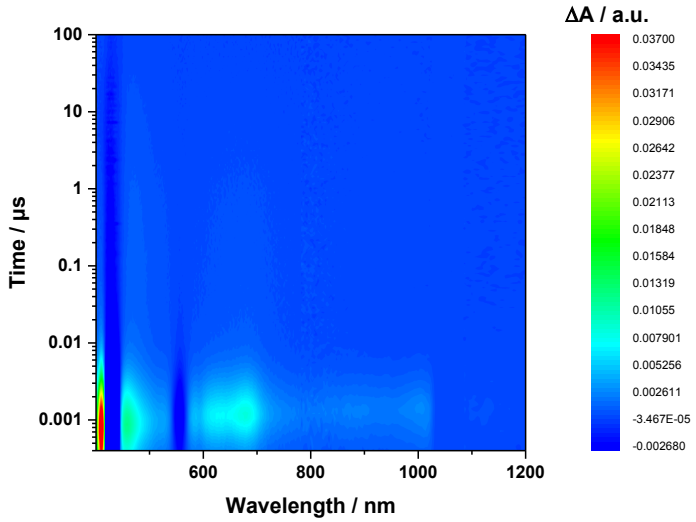

Figure S6: Contour plot of the transient absorption measurements of **1Zn** in chlorobenzene upon excitation with 430 nm laser pulses with time delays from 0.1 ns to 100 µs – please note the detector change at around 900 nm and the probe fundamental at around 1064 nm.

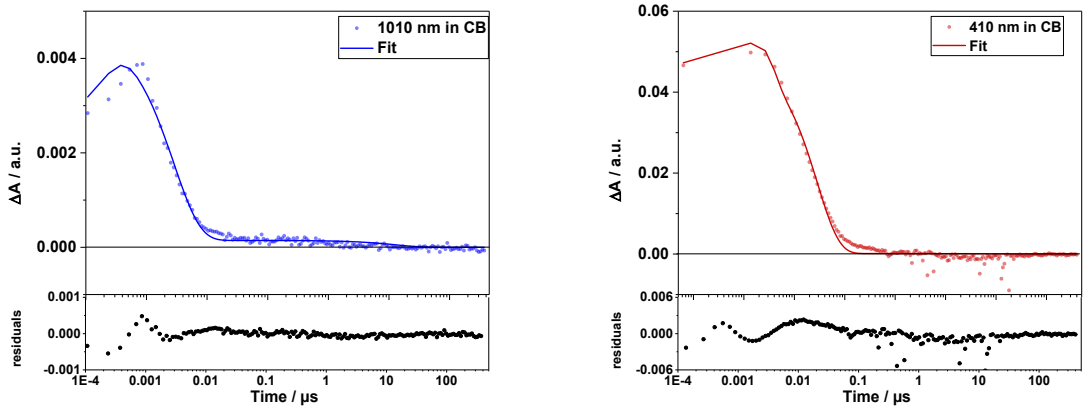

Figure S7: Time traces (dots) and the corresponding fits (lines) of **1Zn** in chlorobenzene. Bottom: fit residuals.

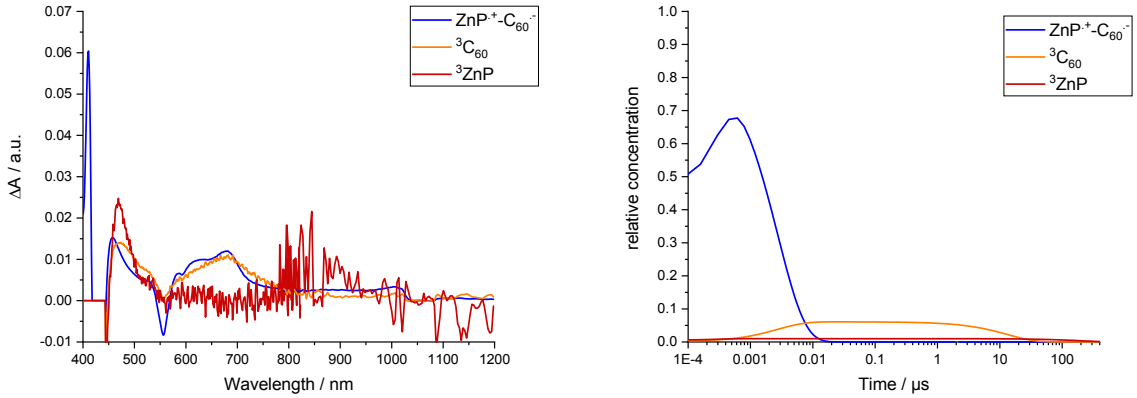

Figure S8: Deconvoluted species associated spectra (SAS) and corresponding concentration profiles of **1Zn** in chlorobenzene depicting the CSS (denoted as $ZnP^{\cdot+}$-$C_{60}^{\cdot-}$) and triplet excited states (denoted as $^{3*}C_{60}$, ^{3*}ZnP) obtained from target analysis.

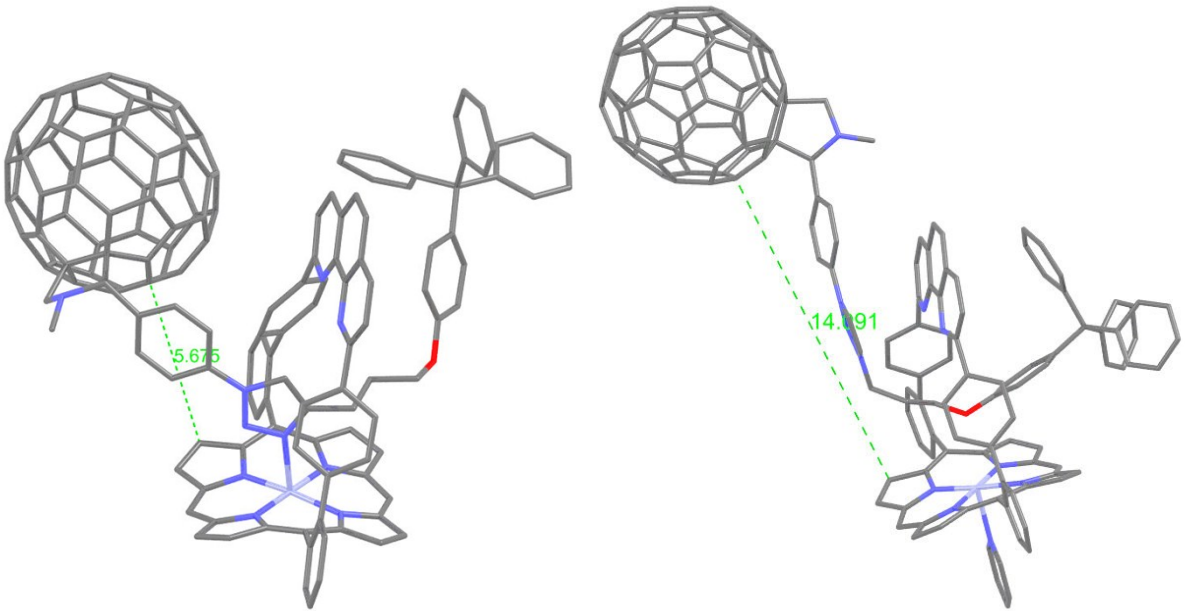

Figure S9: Energy Minimized (Spartan, MM2 level) conformations of the contracted and extended forms of the rotaxane **1Zn** in the absence of pyridine (left) and in the presence of pyridine (right) using restraints to impose the H-bond between the triazole proton (left) and the central methylene group of the dumbbell's propylene chain (right) with the phenanthroline's nitrogen (interactions observed by NMR). The two conformations which show the maximum amplitude of the motion (ca. 8 Å) are in agreement with all the chemical shifts observed in the 1D and 2D ^{1}H NMR. Please note the t-Bu groups of the stopper on the right have been omitted to shorten the calculation time.

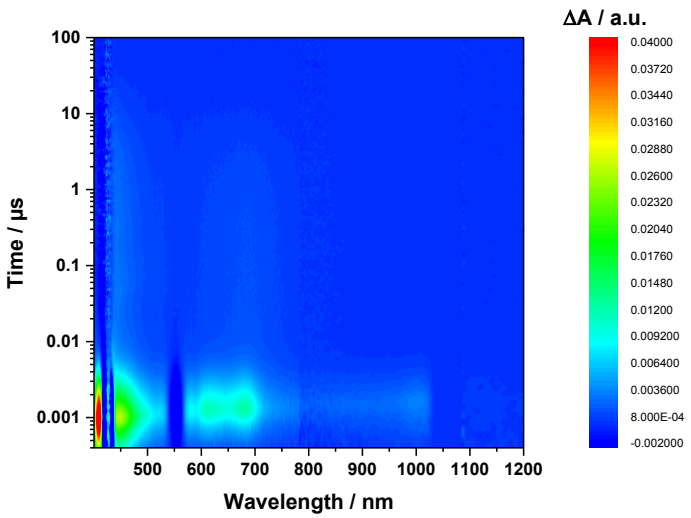

Figure S10: Contour plot of the transient absorption measurements of **1Zn** in toluene with 10^{-3}M pyridine upon excitation with 430 nm laser pulses with time delays from 0.1 ns to 100 µs – please note the detector change at around 900 nm and the probe fundamental at around 1064 nm.

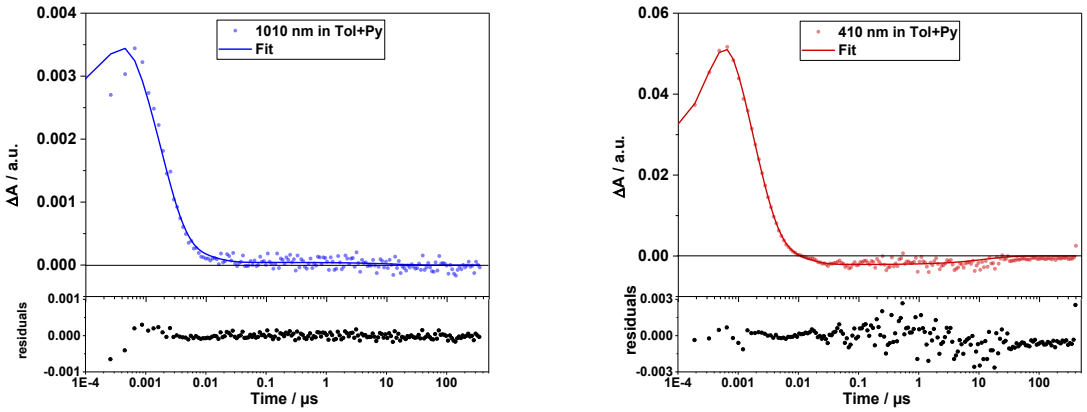

Figure S11: Time traces (dots) and the corresponding fits (lines) of **1Zn** in toluene with added pyridine. Bottom: fit residuals.

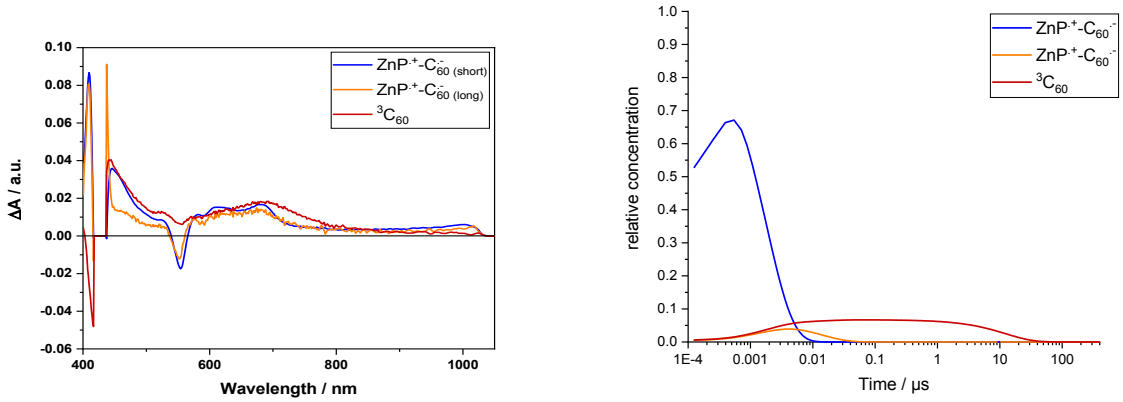

Figure S12: Deconvoluted species associated spectra (SAS) and corresponding concentration profiles of **1Zn** in toluene with added pyridine depicting two CSS with different lifetime (denoted as $ZnP^{\cdot+}$-$C_{60}^{\cdot-}$) and triplet excited state (denoted as $^{3*}C_{60}$) obtained from target analysis.

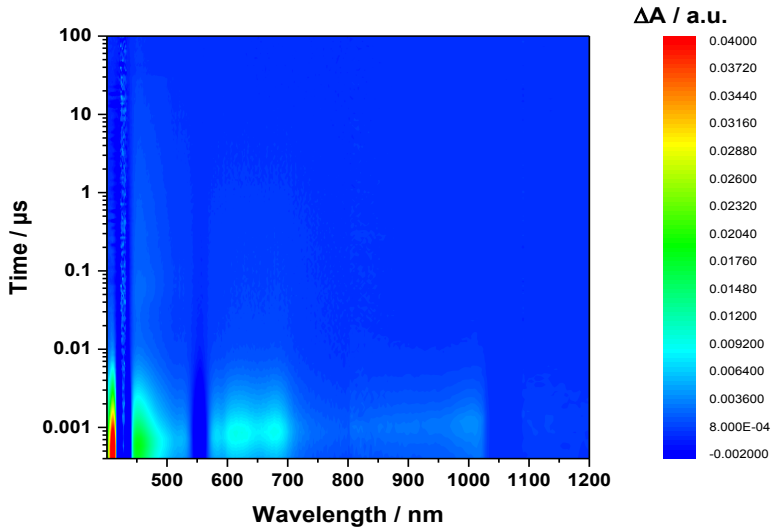

Figure S13: Contour plot of the transient absorption measurements of **1Zn** in chlorobenzene with 10^{-3} M pyridine upon excitation with 430 nm laser pulses with time delays from 0.1 ns to 100 µs – please note the detector change at around 900 nm and the probe fundamental at around 1064 nm.

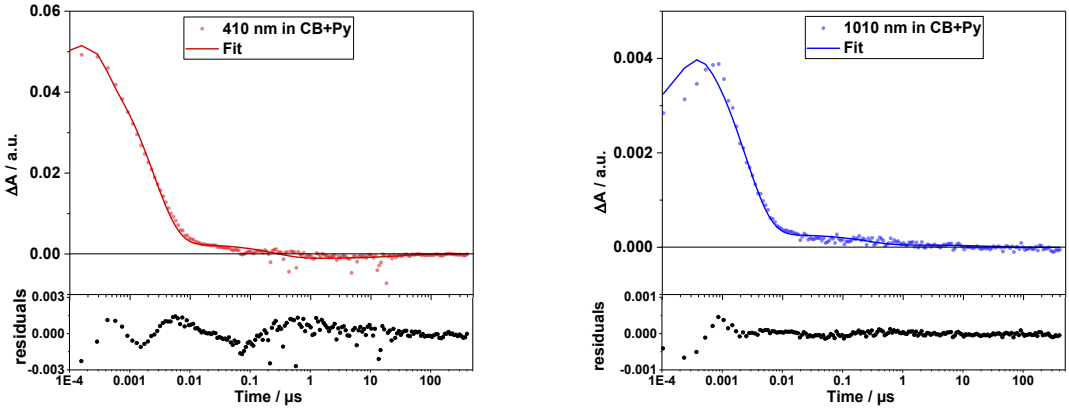

Figure S14: Time traces (dots) and the corresponding fits (lines) of **1Zn** in chlorobenzene with added pyridine. Bottom: fit residuals.

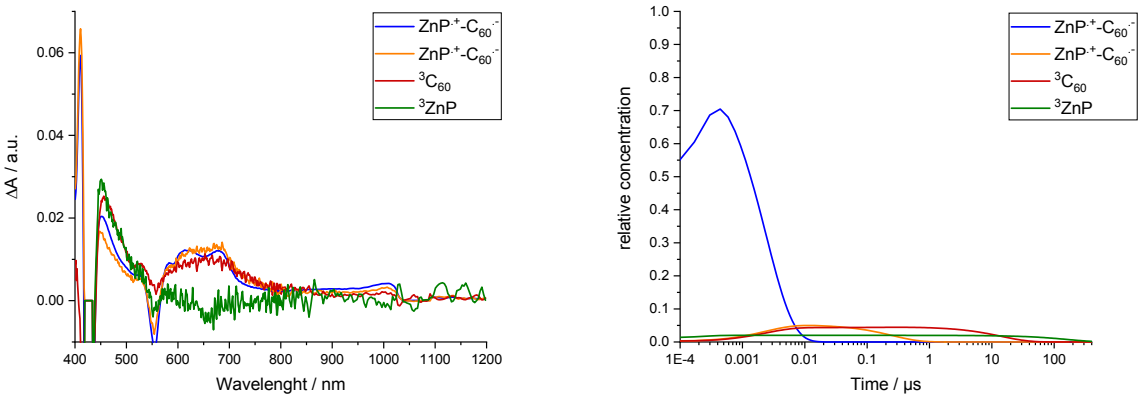

Figure S15: Deconvoluted species associated spectra (SAS) and corresponding concentration profiles of **1Zn** in chlorobenzene with added pyridine depicting two CSS with different lifetime (denoted as $ZnP^{\cdot+}$-$C_{60}^{\cdot-}$) and triplet excited states (denoted as $^{3*}C_{60}$, $^{3*}ZnP$) obtained from target analysis.

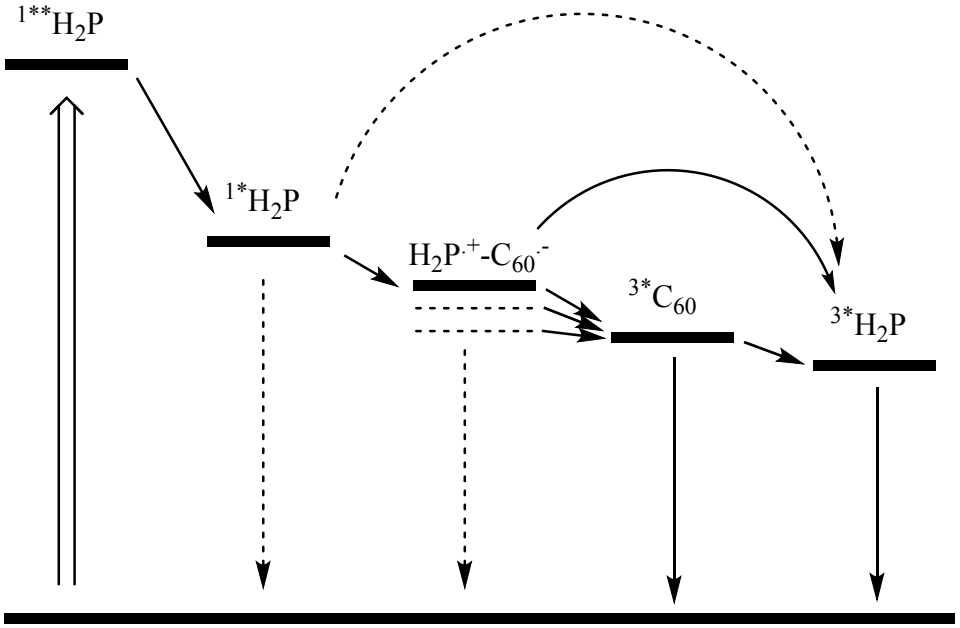

Figure S16: Summary of the possible deactivation pathways for **1**.

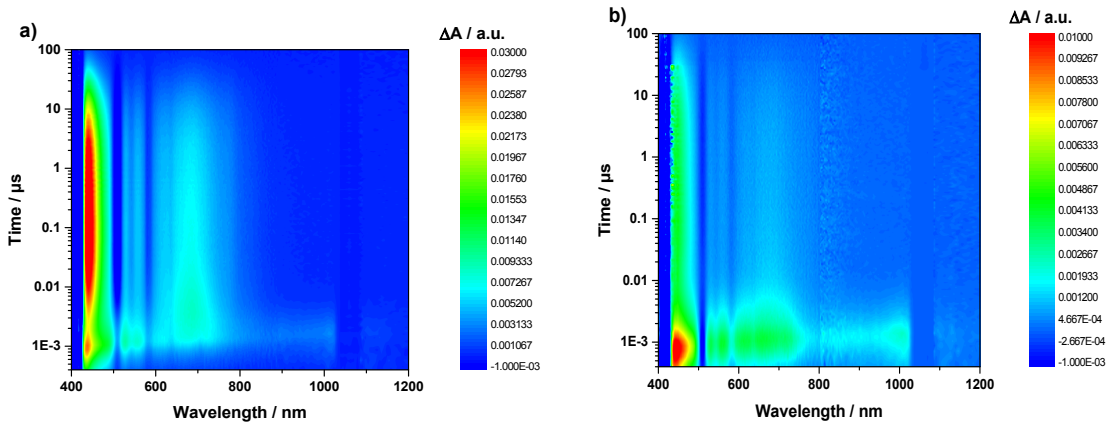

Figure S17: Contour plots of the transient absorption measurements of **1** in a) toluene and b) benzonitrile upon excitation with 430 nm pulses with time delays from 0.1 ns to 100 µs – please note the detector change at around 900 nm and the probe fundamental at around 1064 nm.

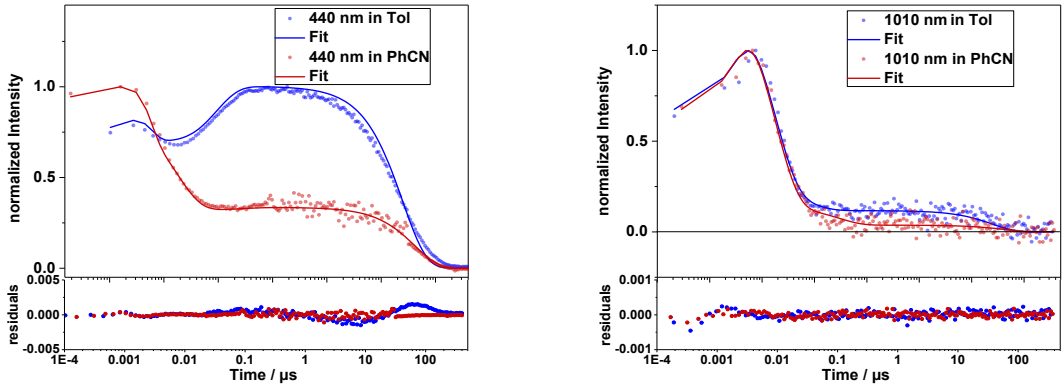

Figure S18: Time traces (dots) and the corresponding fits (lines) of **1** in toluene and benzonitrile. Bottom: fit residuals.

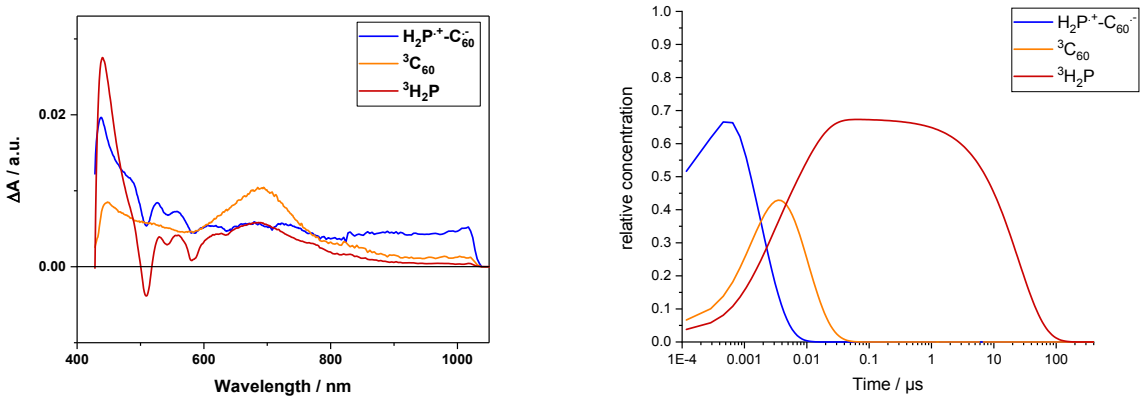

Figure S19: Species associated spectra (SAS) and corresponding concentration profiles of **1** in toluene depicting the CSS (denoted as $H_2P^{\cdot+}$-$C_{60}^{\cdot-}$) and triplet excited states (denoted as $^{3*}C_{60}$ and $^{3*}H_2P$) obtained from target analysis.

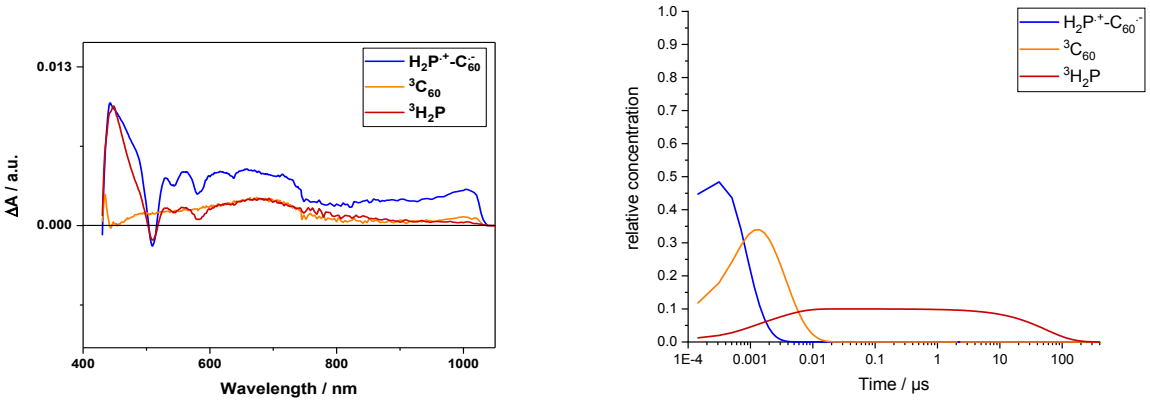

Figure S20: Species associated spectra (SAS) and corresponding concentration profiles of **1** in benzonitrile depicting the CSS (denoted as $H_2P^{\cdot+}$-$C_{60}^{\cdot-}$) and triplet excited states (denoted as $^{3*}C_{60}$ and $^{3*}H_2P$) obtained from target analysis.

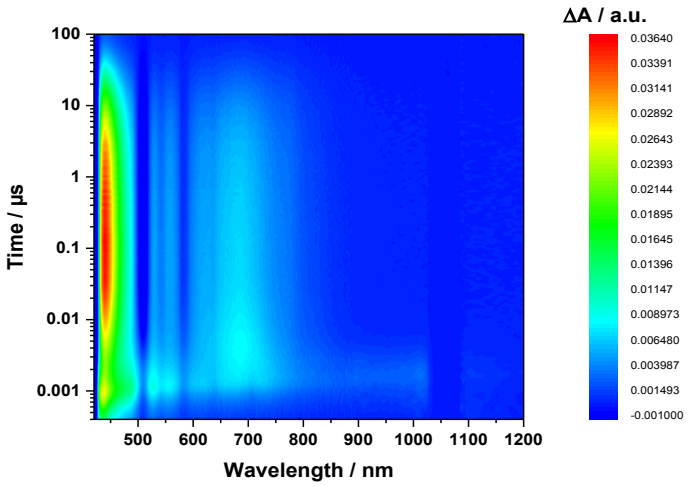

Figure S21: Contour plot of the transient absorption measurements of **1** in toluene with 10^{-3} M pyridine upon excitation with 430 nm pulses with time delays from 0.1 ns to 100 µs – please note the detector change at around 900 nm and the probe fundamental at around 1064 nm.

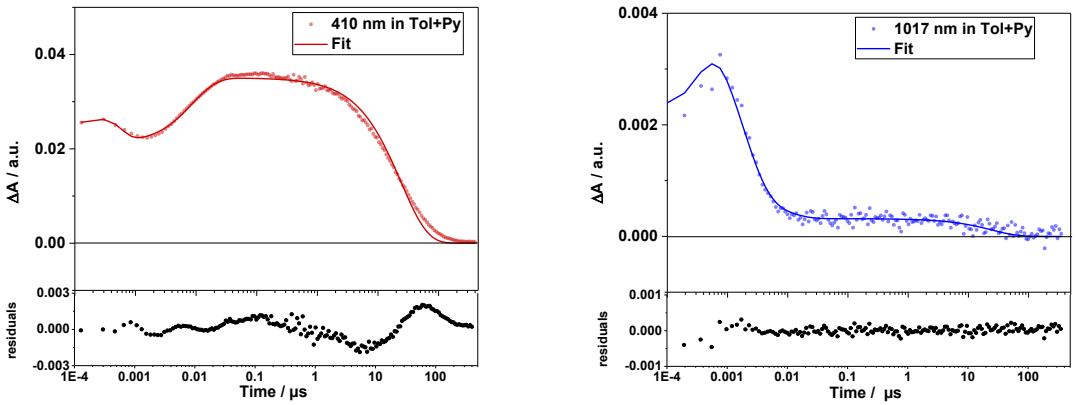

Figure S22: Time traces (dots) and the corresponding fits (lines) of **1** in toluene with added pyridine. Bottom: fit residuals.

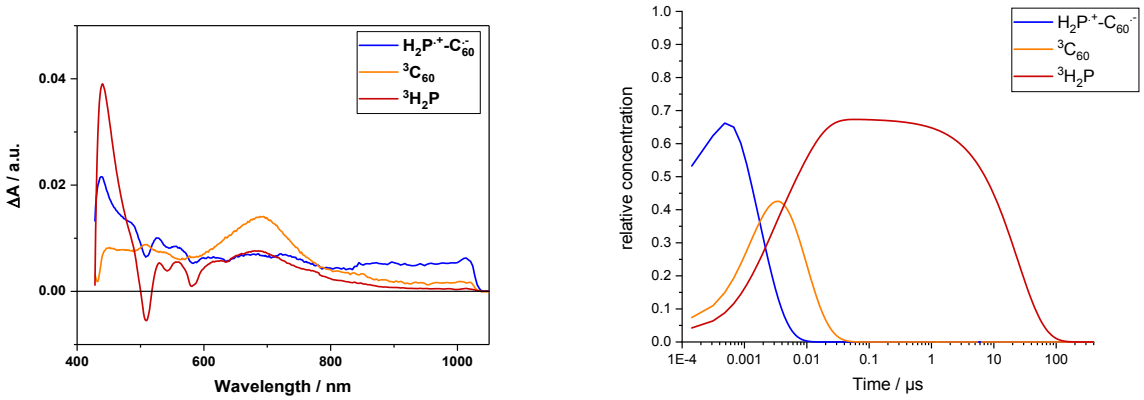

Figure S23: Species associated spectra (SAS) and corresponding concentration profiles of **1** in toluene with added pyridine depicting the CSS (denoted as $H_2P^{\cdot+}$-$C_{60}^{\cdot-}$) and triplet excited states (denoted as $^{3*}C_{60}$ and $^{3*}H_2P$) obtained from target analysis.

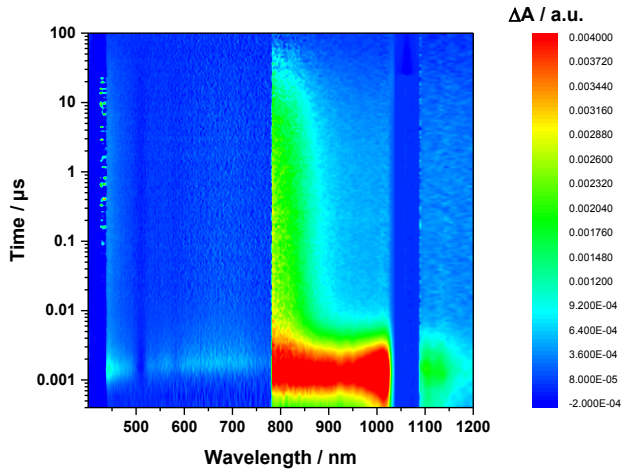

Figure S24: Contour plot of the transient absorption measurements of **1** in chlorobenzene with 10^{-3} M pyridine upon excitation with 430 nm pulses with time delays from 0.1 ns to 100 µs – please note the detector change at around 900 nm and the probe fundamental at around 1064 nm.

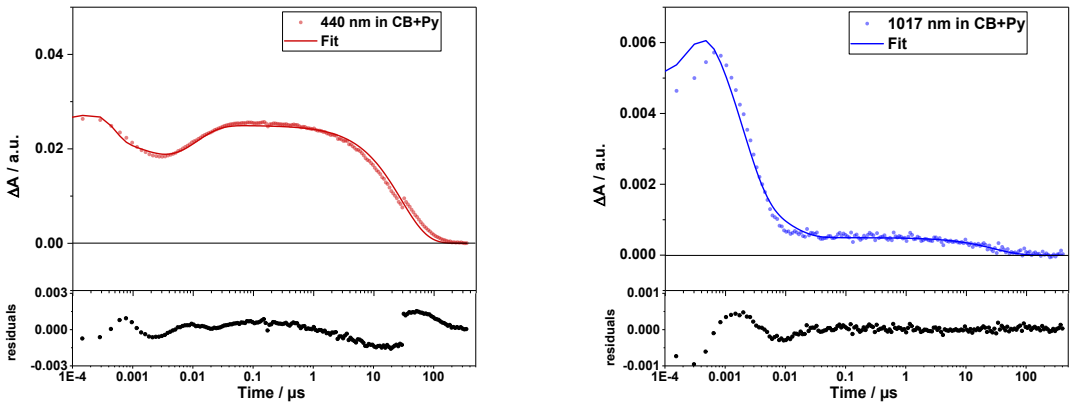

Figure S25: Time traces (dots) and the corresponding fits (lines) of **1** in chlorobenzene with added pyridine. Bottom: fit residuals.

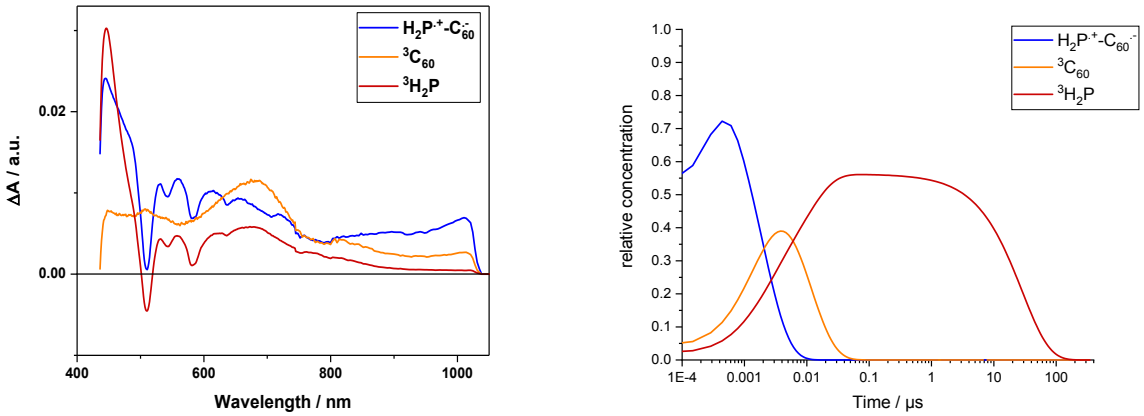

Figure S26: Species associated spectra (SAS) of **1** in chlorobenzene with added pyridine depicting the CSS (denoted as $H_2P^{\cdot+}$-$C_{60}^{\cdot-}$) and triplet excited states (denoted as $^{3*}C_{60}$ and $^{3*}H_2P$) obtained from target analysis.

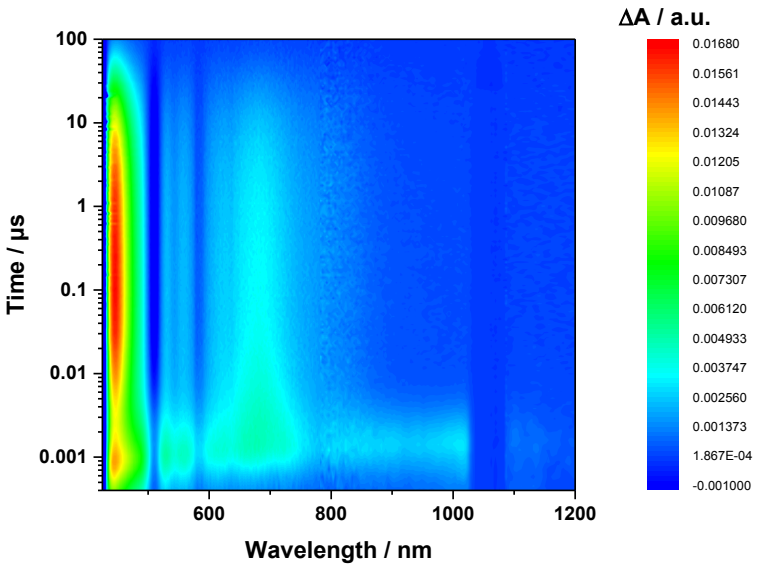

Figure S27: Contour plot of the transient absorption measurements of **1** in chlorobenzene upon excitation with 430 nm pulses with time delays from 0.1 ns to 100 µs – please note the detector change at around 900 nm and the probe fundamental at around 1064 nm.

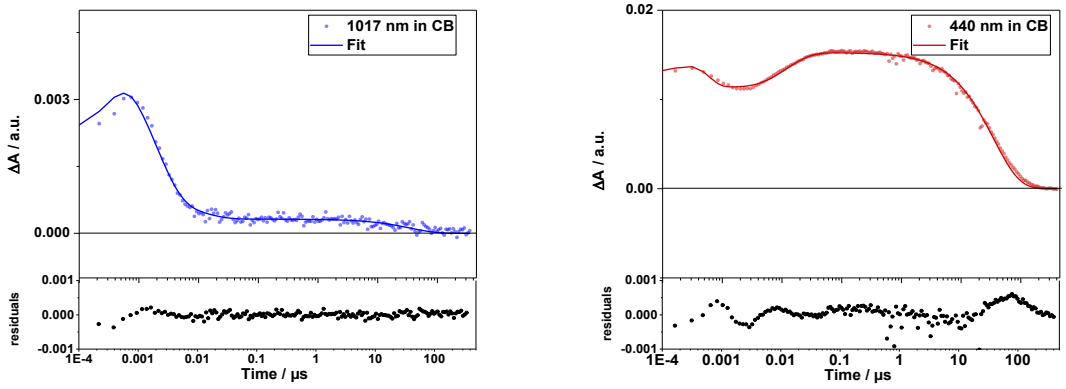

Figure S28: Time traces (dots) and the corresponding fits (lines) of **1** in chlorobenzene. Bottom: fit residuals.

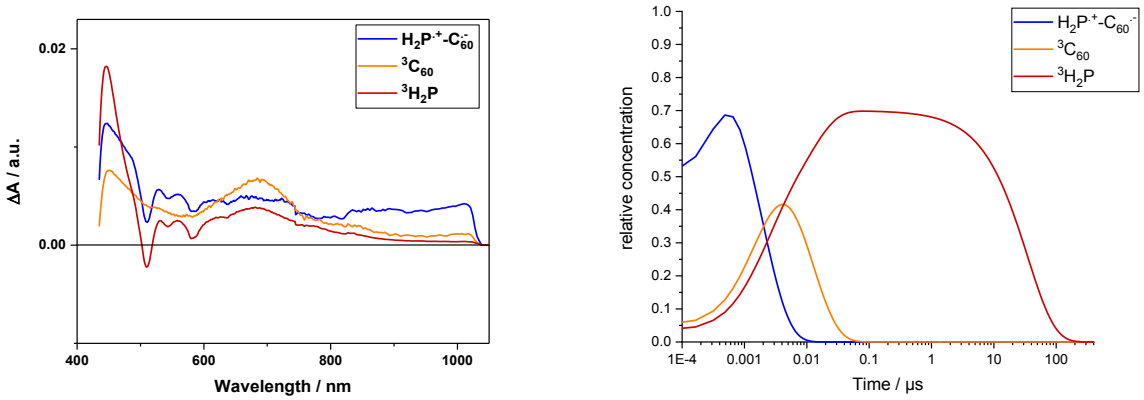

Figure S29: Species associated spectra (SAS) and corresponding concentration profiles of **1** in chlorobenzene depicting the CSS (denoted as $H_2P^{\cdot+}$-$C_{60}^{\cdot-}$) and triplet excited states (denoted as $^{3*}C_{60}$ and $^{3*}H_2P$) obtained from target analysis.

Table S3: Summary of excited state lifetimes determined by means of GTA for **1** in various solvents.

	toluene	toluene + pyridine	chlorobenzene	chlorobenzene + pyridine	benzonitrile
$^{1**}H_2P$ / ps	0.86	2.00	1.81	2.00	0.80
$^{1*}H_2P$ / ps	24.7	30.0	36.0	30.0	46.9
$(H_2P^{\cdot+}\text{-}C_{60}^{\cdot-})$ / ns	1.77	1.72	1.91	1.85	1.80
$^{3*}C_{60}$ / ns	8.58	8.00	11.2	10.1	29.7
$^{3*}H_2P$ / µs	24.8	24.1	34.9	28.6	41.8

Despite significantly smaller driving forces of CS in **1** vs **1Zn**, formation of the CSS is nearly as fast in **1** as in **1Zn**. No solvent or solvent combination induces multiple components in the observed CSS lifetimes. As in **1Zn**, this indicates no coexistence of triplet CSS parallel to the singlet CSS originating from $^{1*}H_2P$. Furthermore, the absence of a metal center in **1** precludes any kind of control over molecular motion in the free base rotaxane. The observed lifetimes of CS suggest closer distances between C_{60} and porphyrin in **1** vs **1Zn** prior to CS, which is likely due to attractive π- π.interactions between C_{60} and H_2P and its phenanthroline strap.

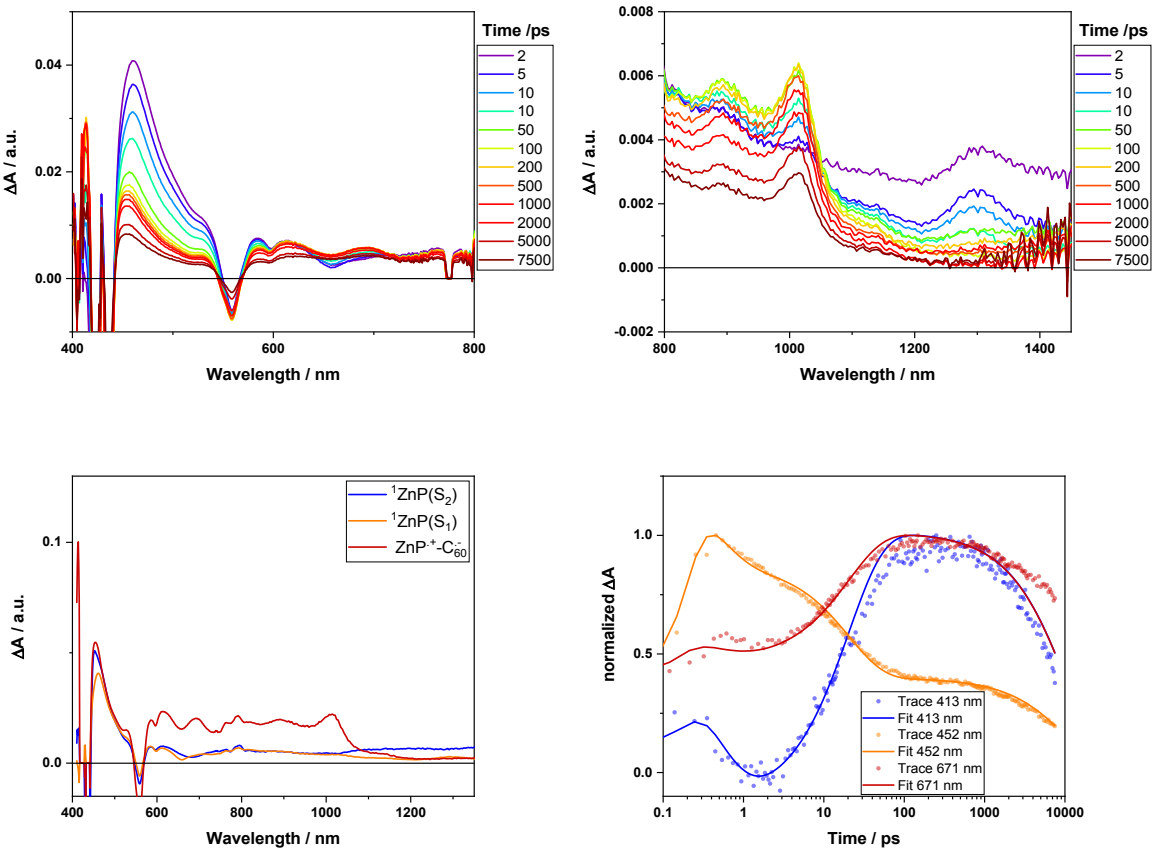

Figure S30: top: time-resolved transient spectra in the visible (left) and near infrared (right) of **1Zn** on the sub-pico- to nanosecond time scale in toluene upon excitation with 430 nm pulses; bottom left: species associated spectra as derived from GloTarAn; bottom right: kinetics and fits at selected wavelengths

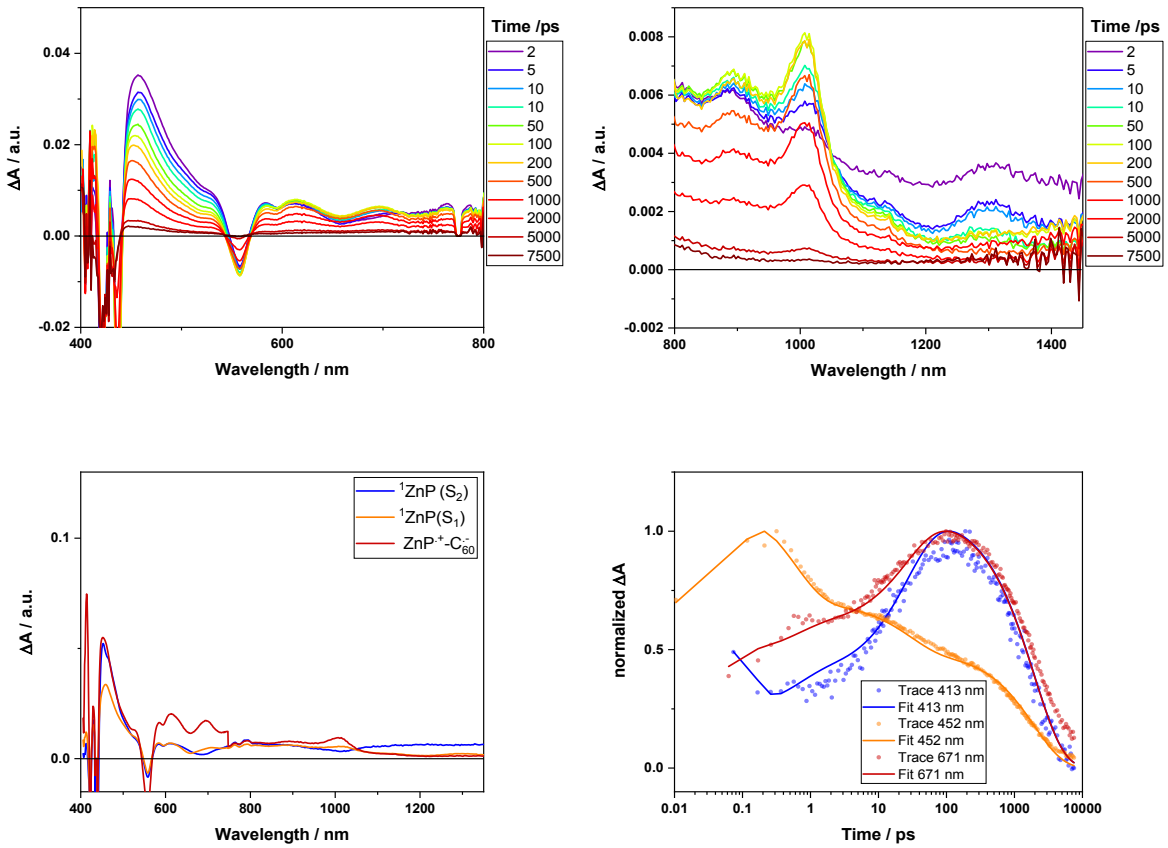

Figure S31: top: time-resolved transient spectra in the visible (left) and near infrared (right) of **1Zn** on the sub-pico- to nanosecond time scale in toluene + pyridine upon excitation with 430 nm pulses; bottom left: species associated spectra as derived from GloTarAn; bottom right: kinetics and fits at selected wavelengths

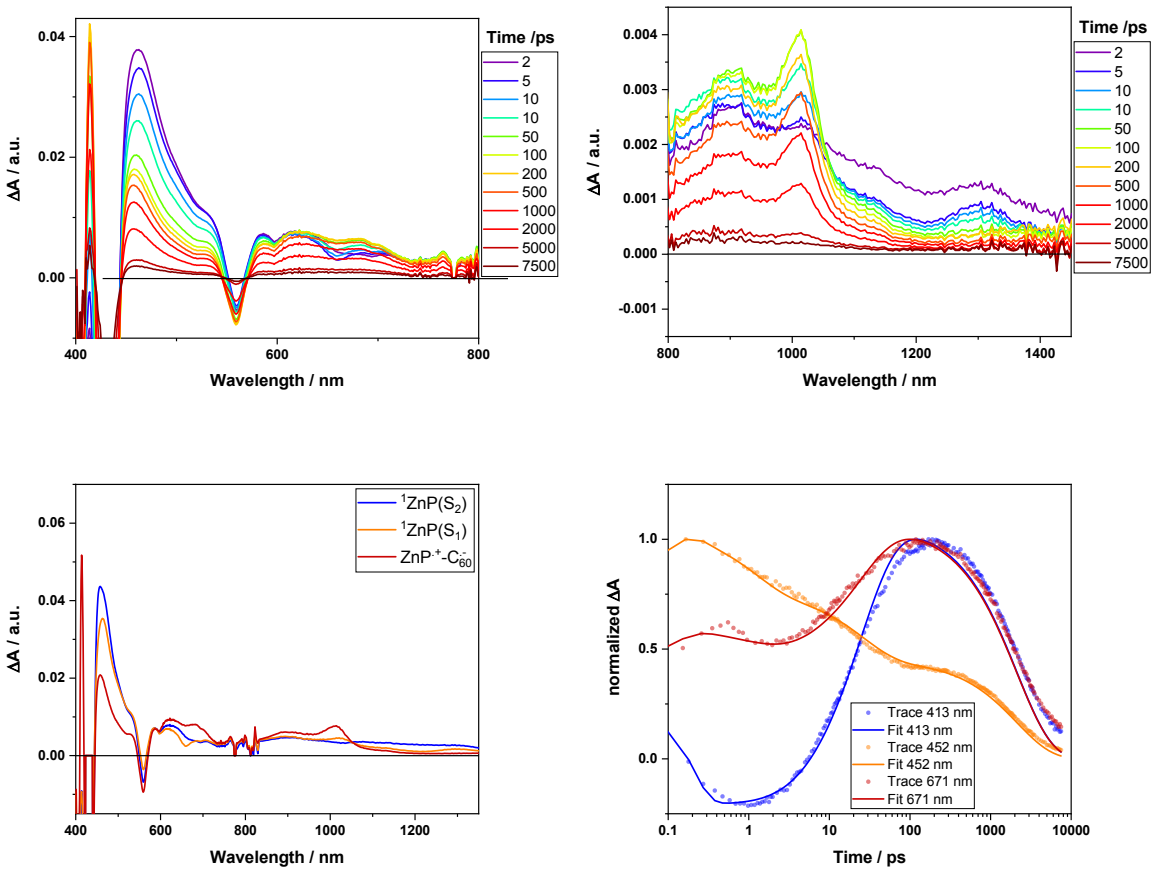

Figure S32: top: time-resolved transient spectra in the visible (left) and near infrared (right) of **1Zn** on the sub-pico- to nanosecond time scale in chlorobenzene upon excitation with 430 nm pulses; bottom left: species associated spectra as derived from GloTarAn; bottom right: kinetics and fits at selected wavelengths

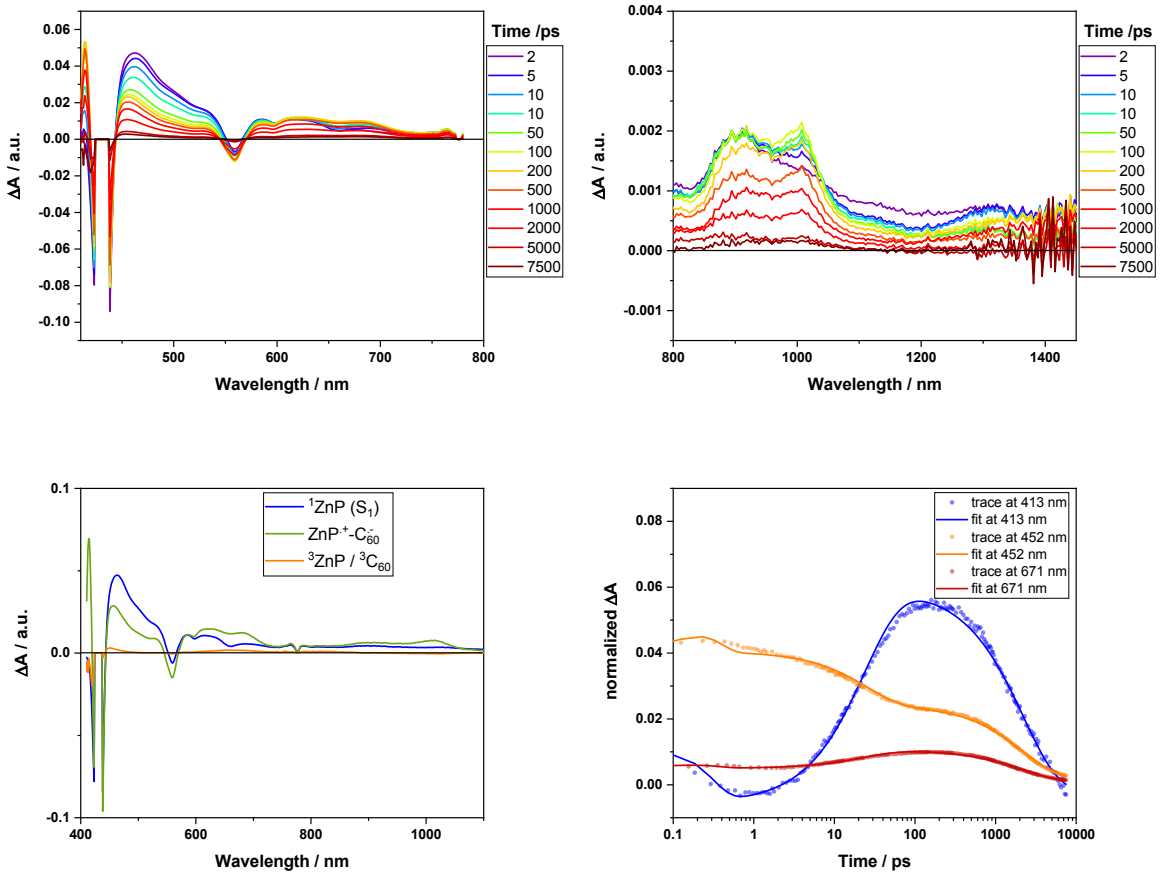

Figure S33: top: time-resolved transient spectra in the visible (left) and near infrared (right) of **1Zn** on the sub-pico- to nanosecond time scale in chlorobenzene + pyridine upon excitation with 430 nm pulses; bottom left: species associated spectra as derived from GloTarAn; bottom right: kinetics and fits at selected wavelengths

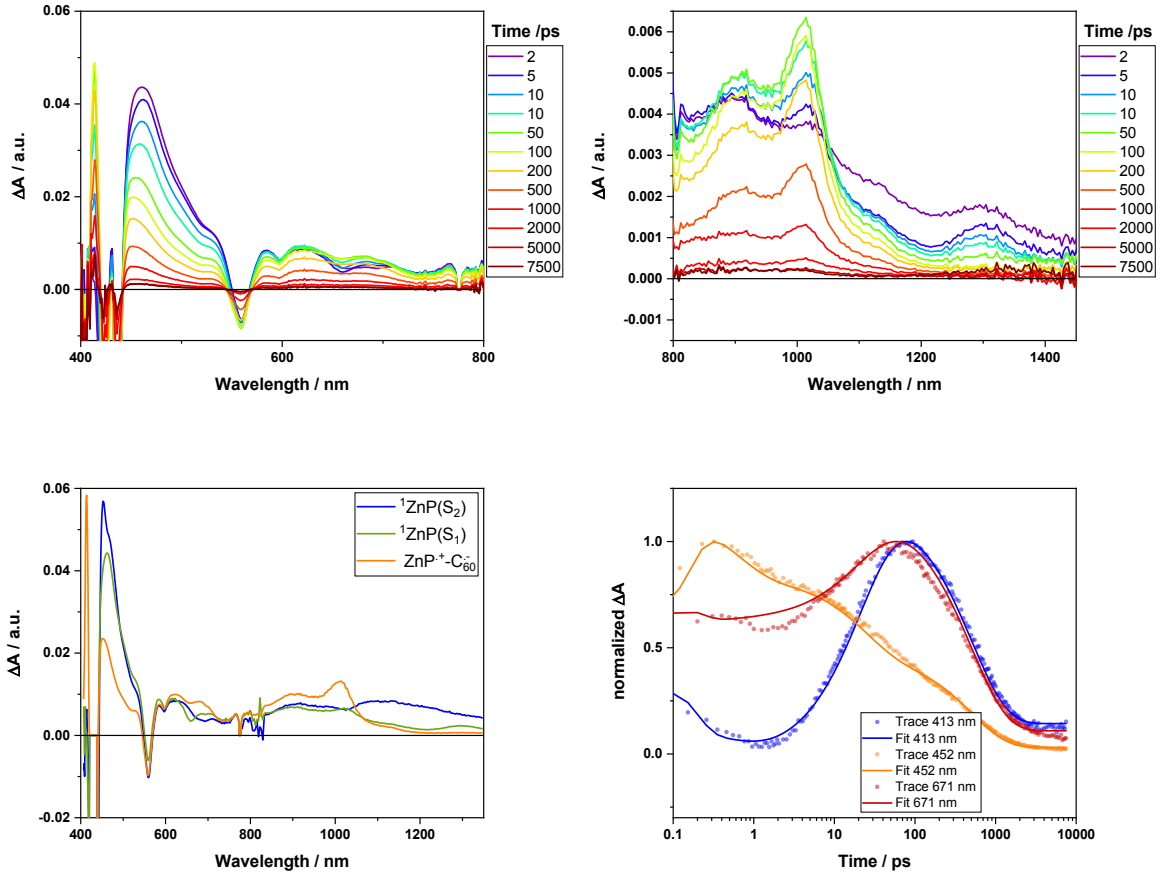

Figure S34: top: time-resolved transient spectra in the visible (left) and near infrared (right) of **1Zn** on the sub-pico- to nanosecond time scale in benzonitrile upon excitation with 430 nm pulses; bottom left: species associated spectra as derived from GloTarAn; bottom right: kinetics and fits at selected wavelengths

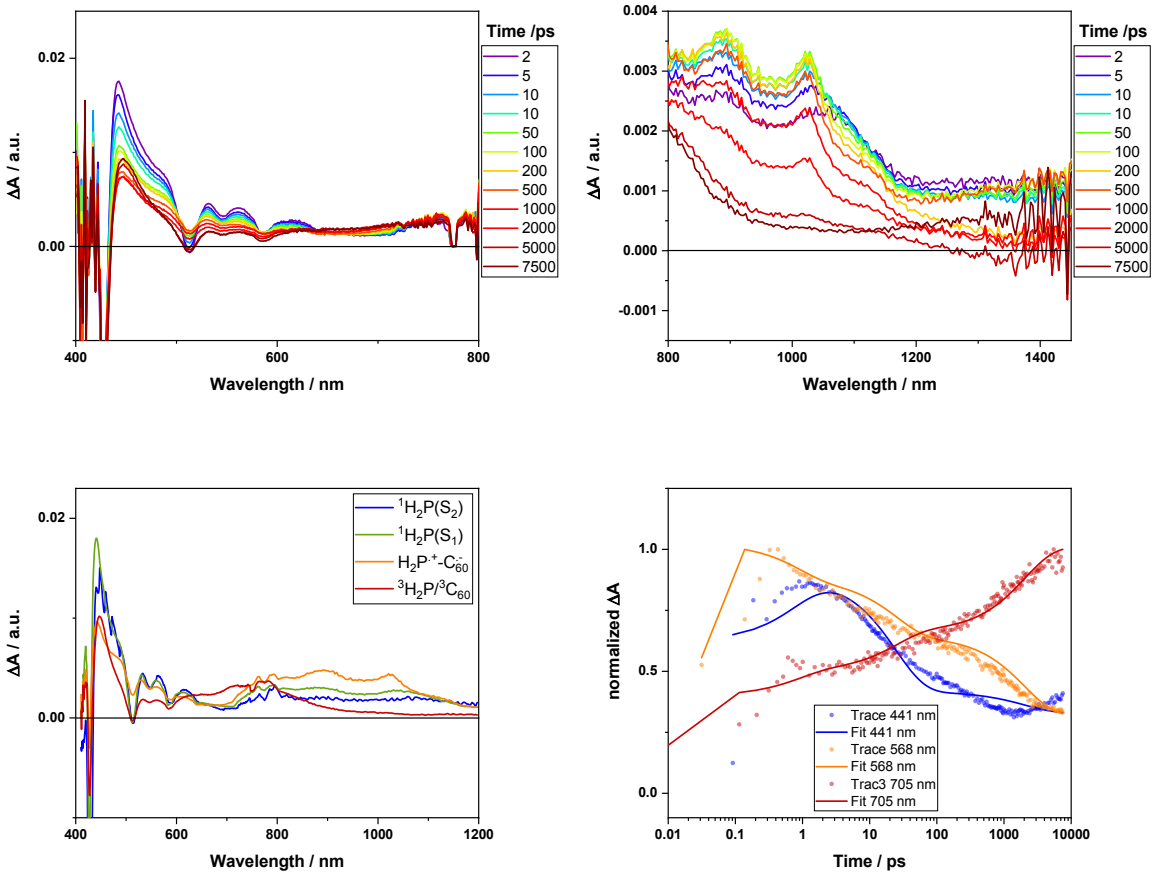

Figure S35: top: time-resolved transient spectra in the visible (left) and near infrared (right) of **1** on the sub-pico- to nanosecond time scale in toluene upon excitation with 430 nm pulses; bottom left: species associated spectra as derived from GloTarAn; bottom right: kinetics and fits at selected wavelengths

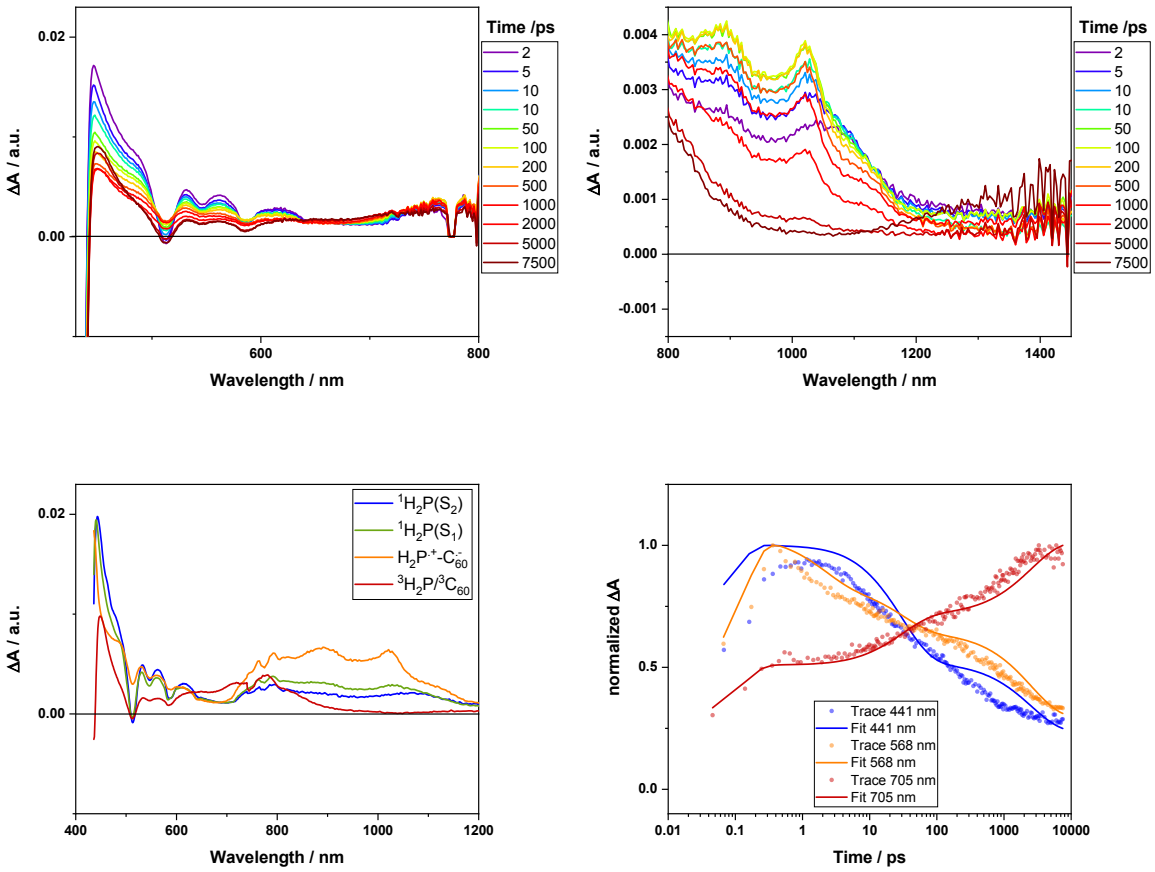

Figure S36: top: time-resolved transient spectra in the visible (left) and near infrared (right) of **1** on the sub-pico- to nanosecond time scale in toluene + pyridine upon excitation with 430 nm pulses; bottom left: species associated spectra as derived from GloTarAn; bottom right: kinetics and fits at selected wavelengths

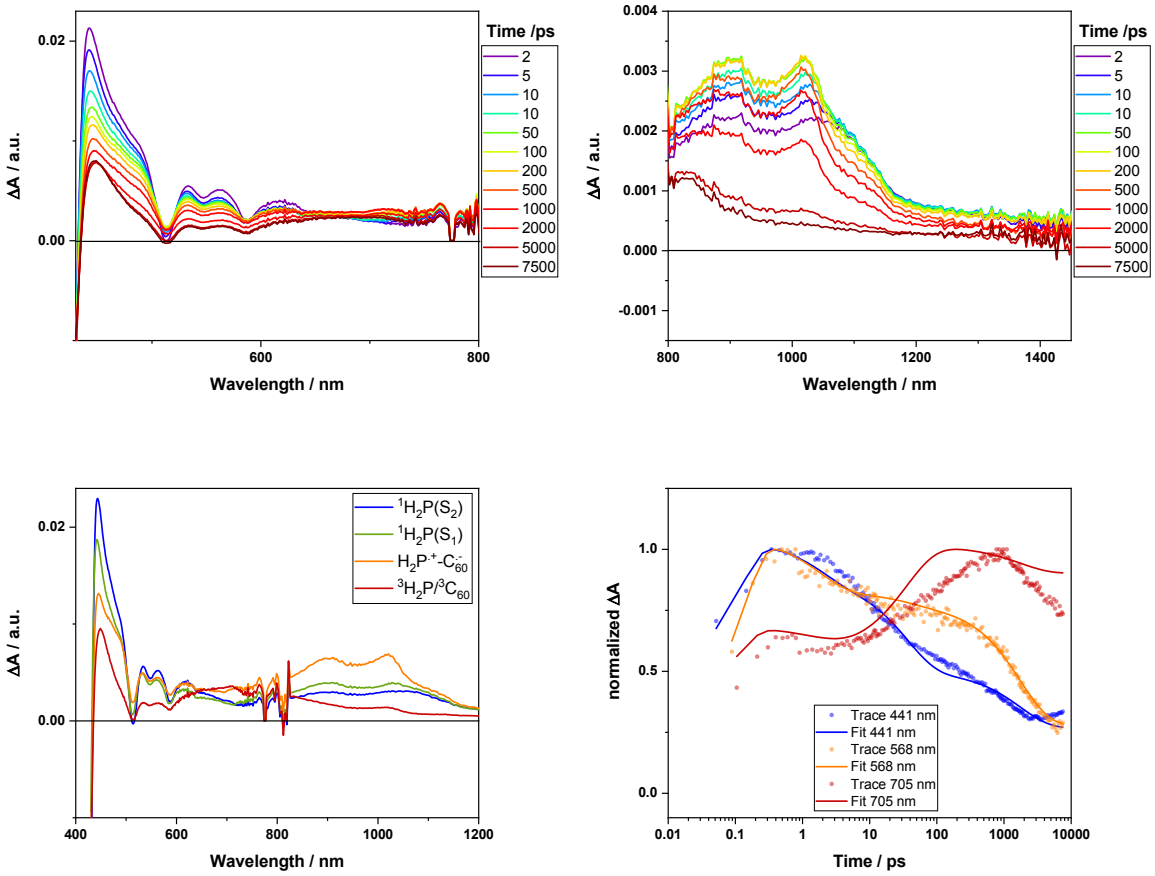

Figure S37: top: time-resolved transient spectra in the visible (left) and near infrared (right) of **1** on the sub-pico- to nanosecond time scale in chlorobenzene upon excitation with 430 nm pulses; bottom left: species associated spectra as derived from GloTarAn; bottom right: kinetics and fits at selected wavelengths

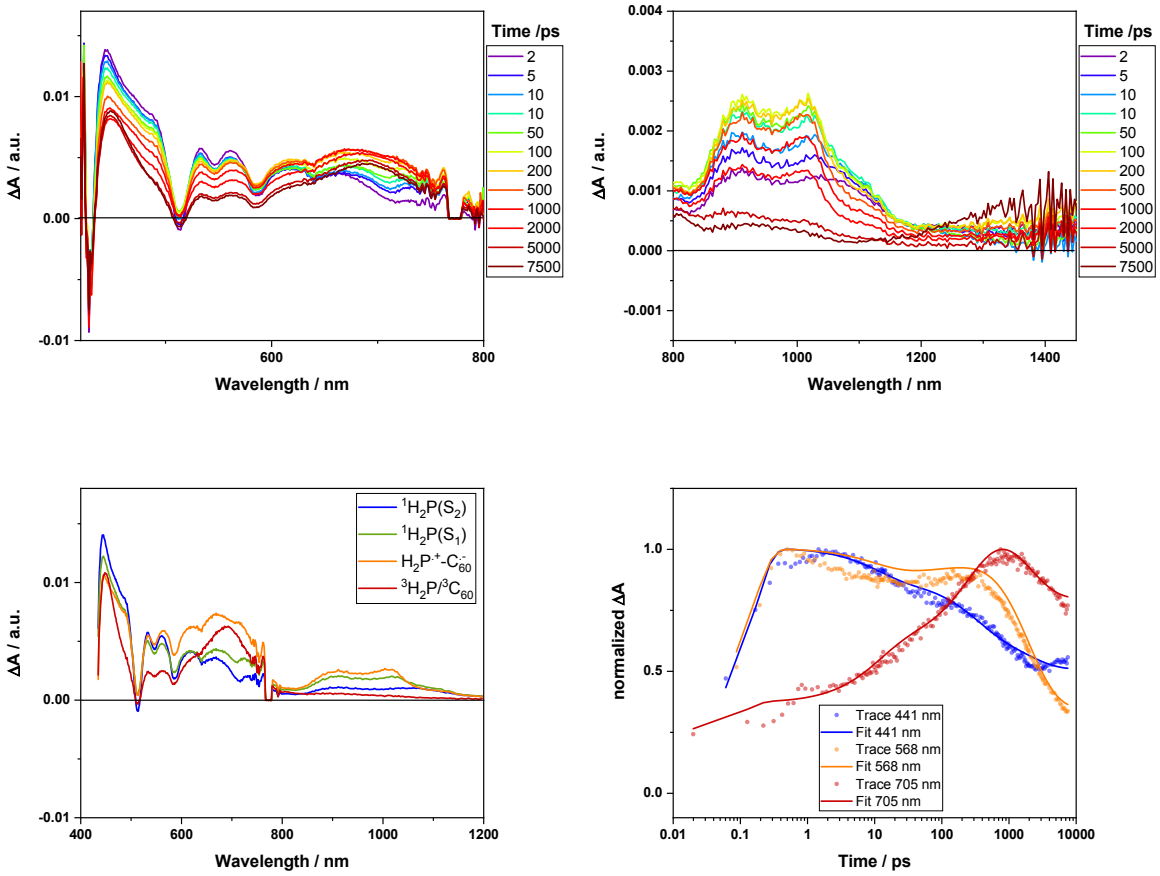

Figure S38: top: time-resolved transient spectra in the visible (left) and near infrared (right) of **1** on the sub-pico- to nanosecond time scale in chlorobenzene + pyridine upon excitation with 430 nm pulses; bottom left: species associated spectra as derived from GloTarAn; bottom right: kinetics and fits at selected wavelengths

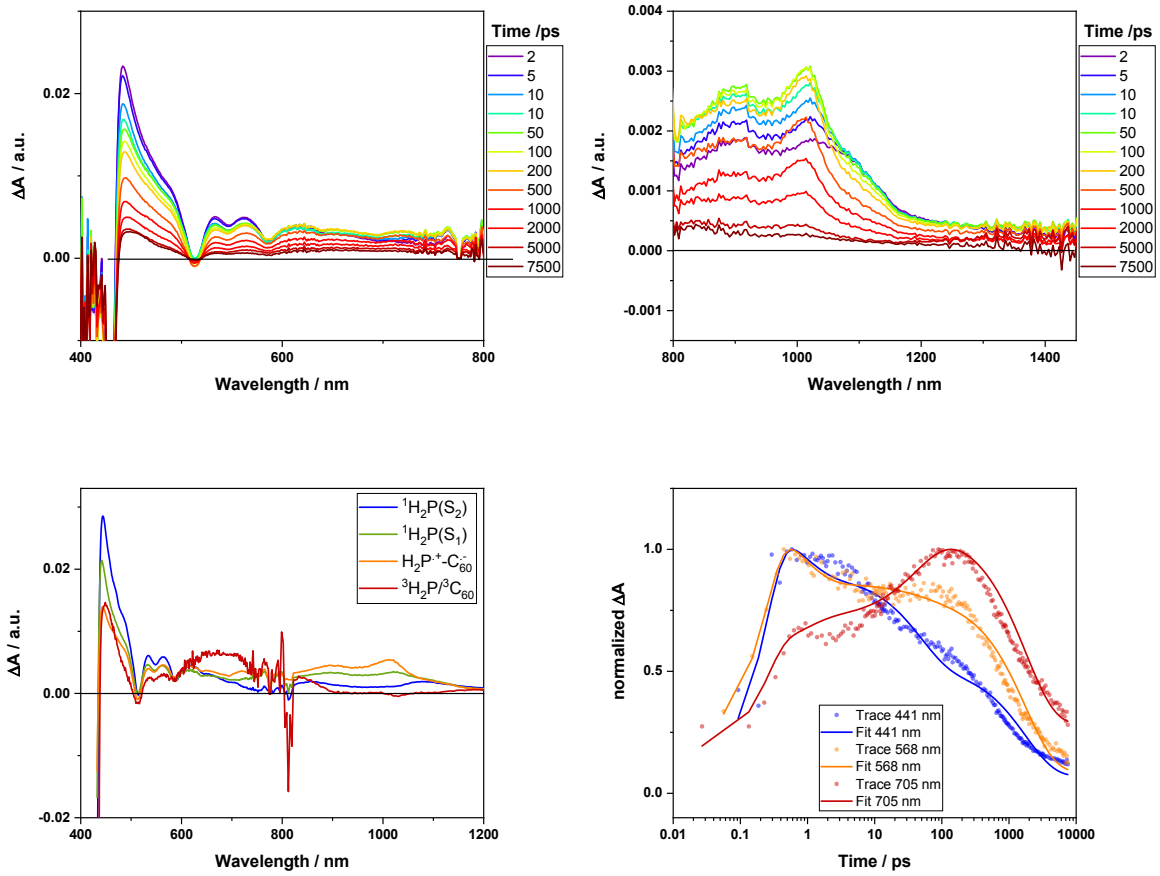

Figure S39: top: time-resolved transient spectra in the visible (left) and near infrared (right) of **1** on the sub-pico- to nanosecond time scale in benzonitrile upon excitation with 430 nm pulses; bottom left: species associated spectra as derived from GloTarAn; bottom right: kinetics and fits at selected wavelengths

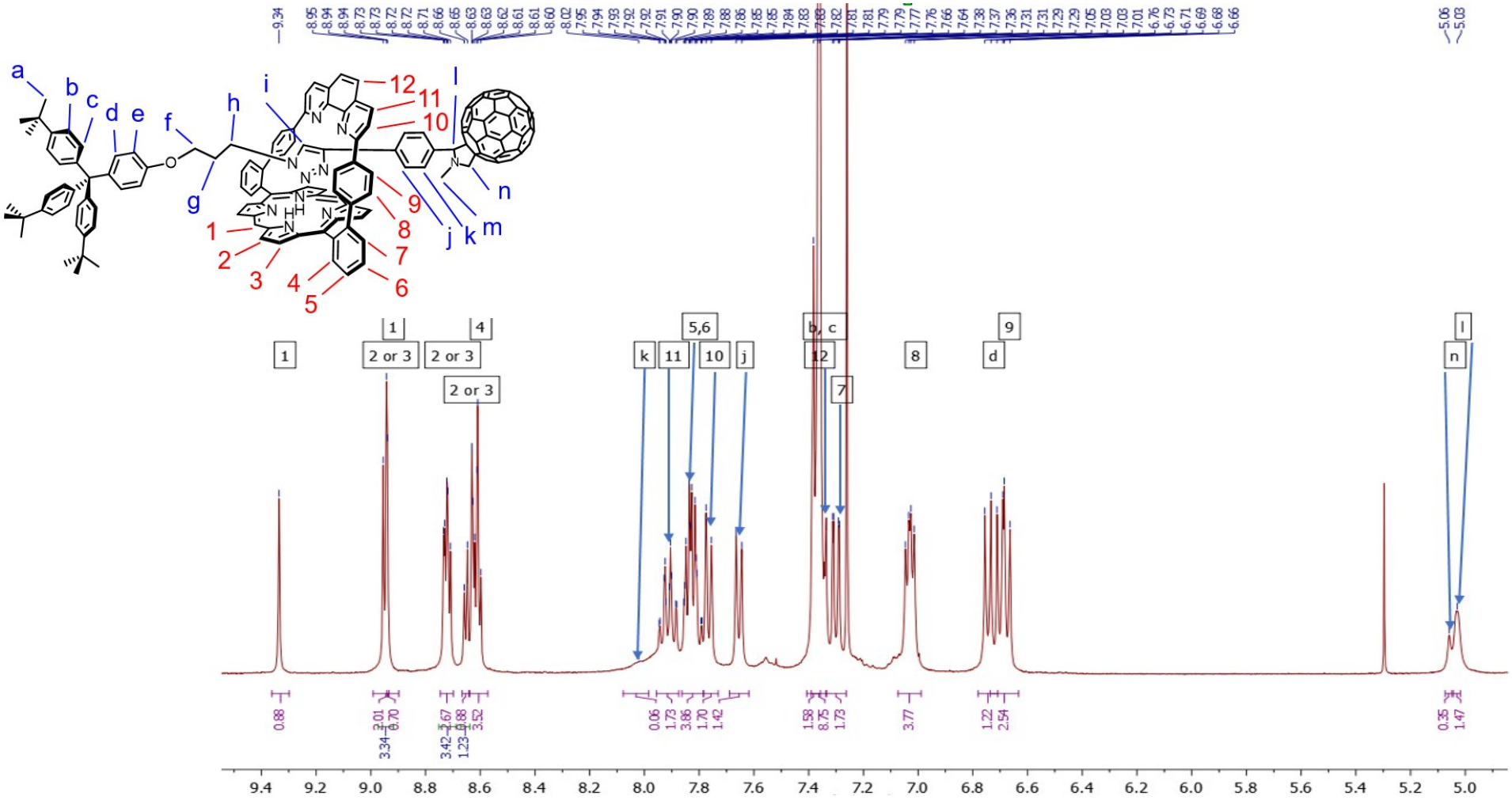

Figure S40: Aromatic region of the ^{1}H NMR spectrum (400 MHz) of **1** in $CDCl_3$.

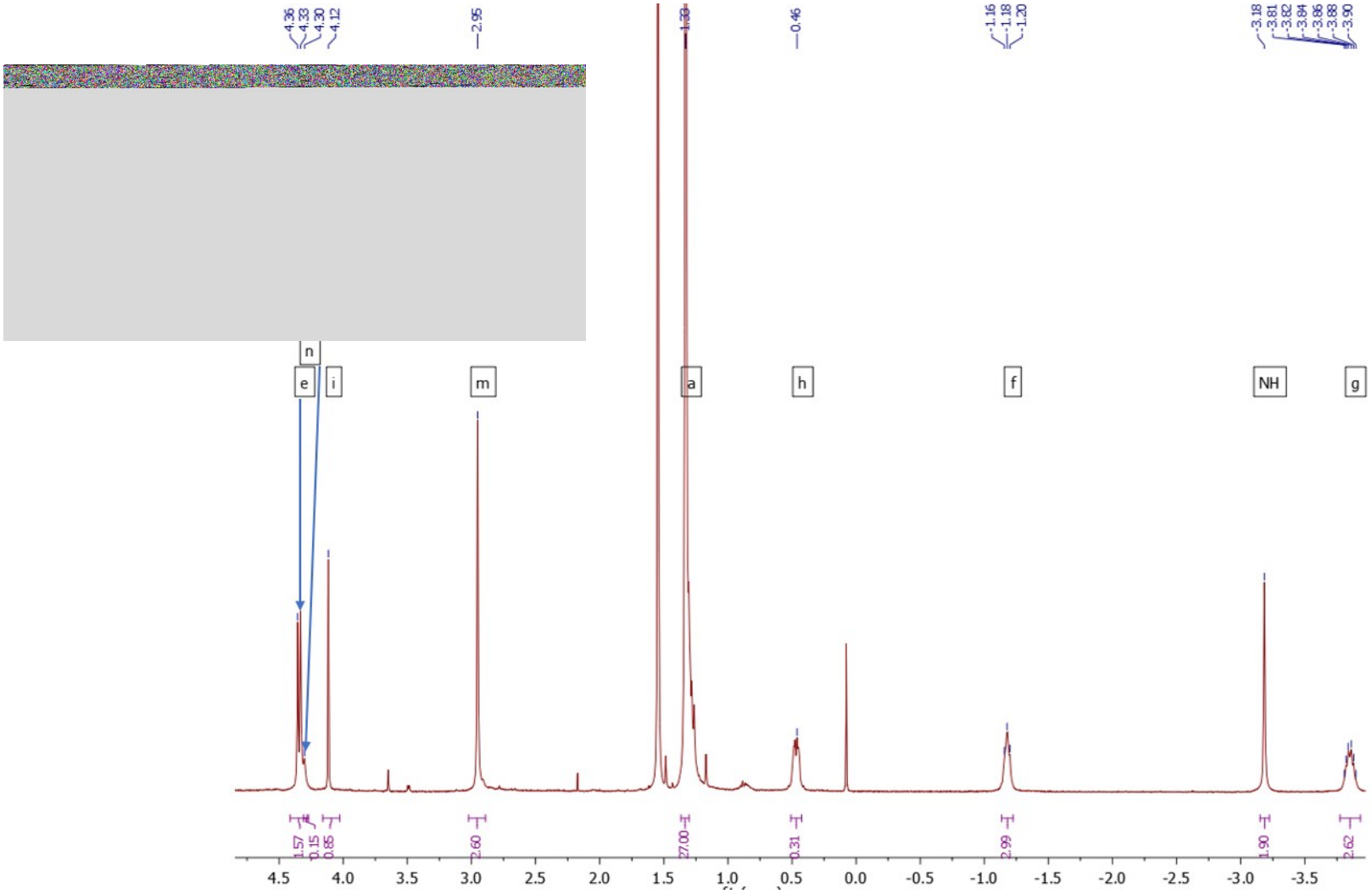

Figure S41: Aliphatic region of the ^{1}H NMR spectrum (400 MHz) of **1** in $CDCl_3$.

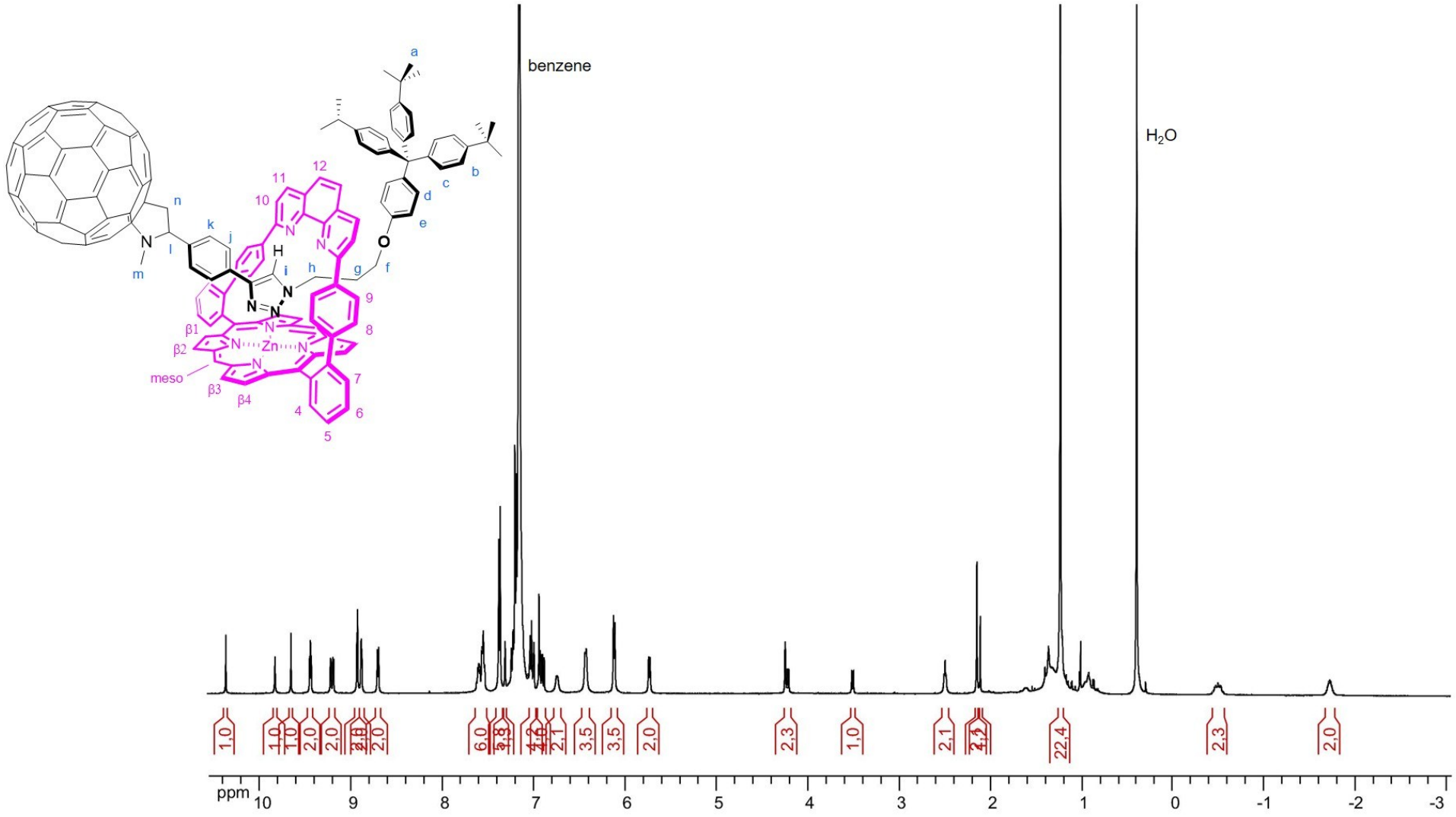

Figure S42: ^{1}H NMR spectrum (500 MHz) of **1Zn** in benzene-d_6.

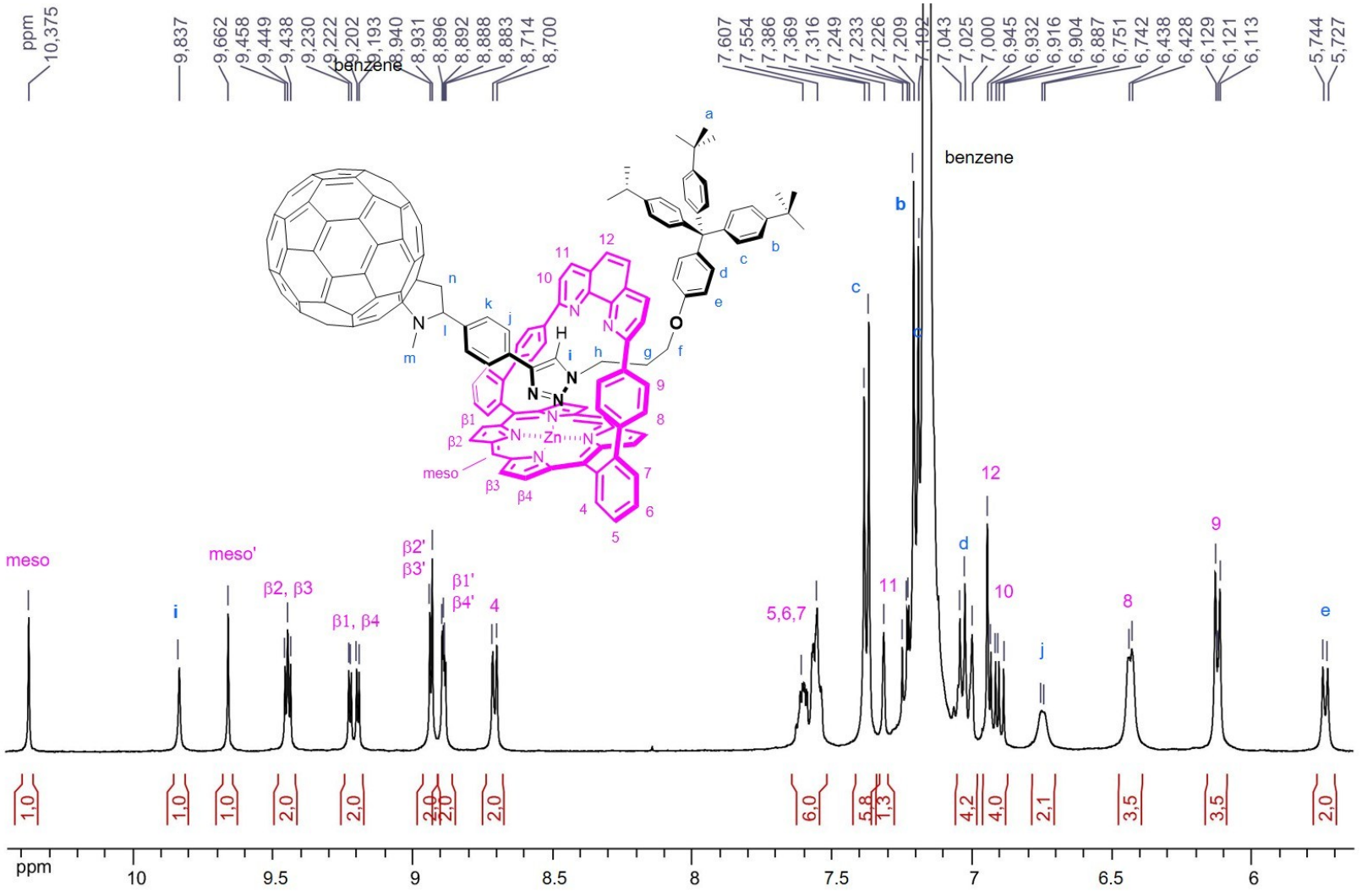

Figure S43: Aromatic region of the ^{1}H NMR spectrum (500 MHz) of **1Zn** in benzene-d_6.

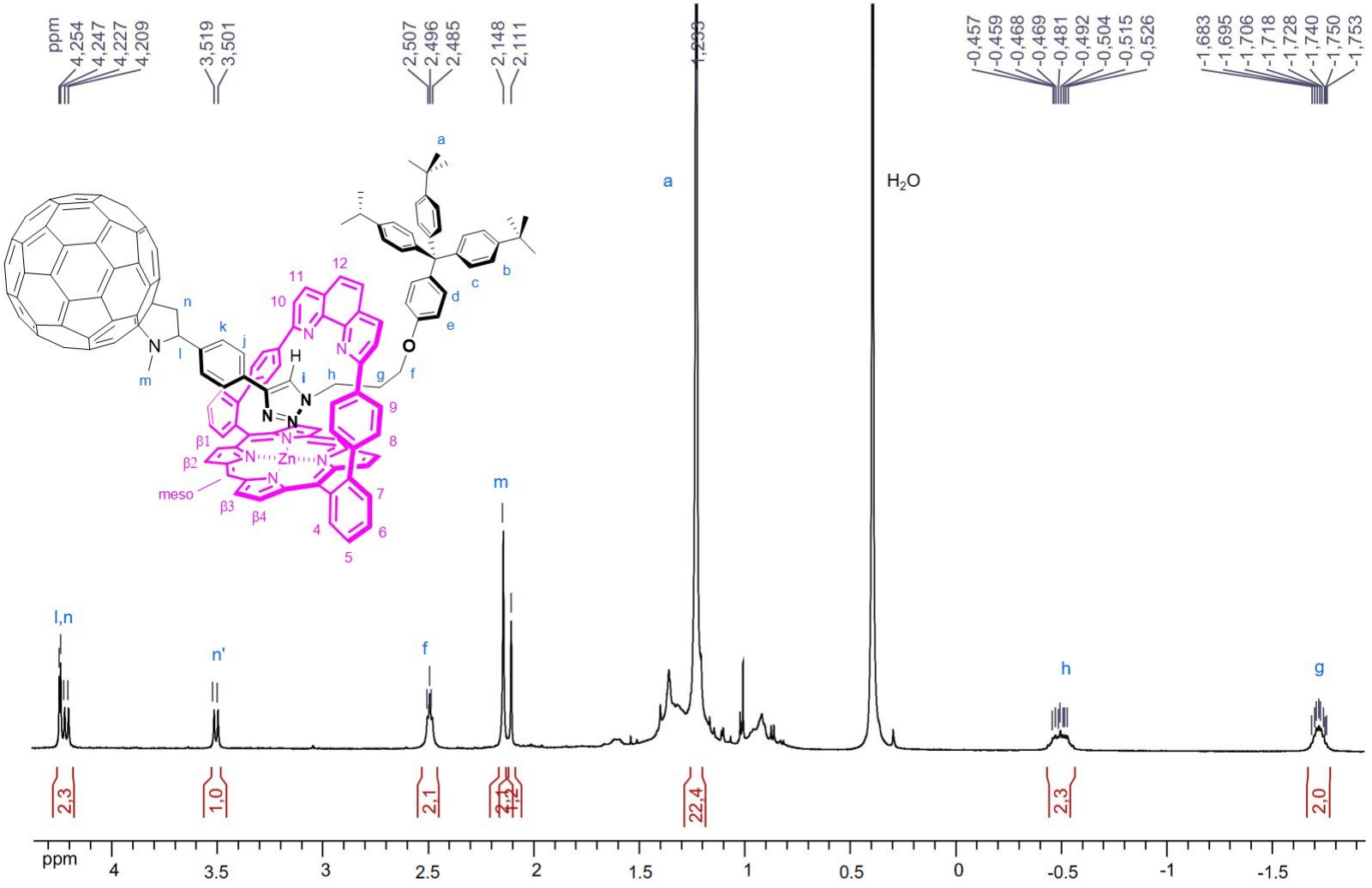

Figure S44: High field region of the ^{1}H NMR spectrum (500 MHz) of **1Zn** in benzene-d_6.

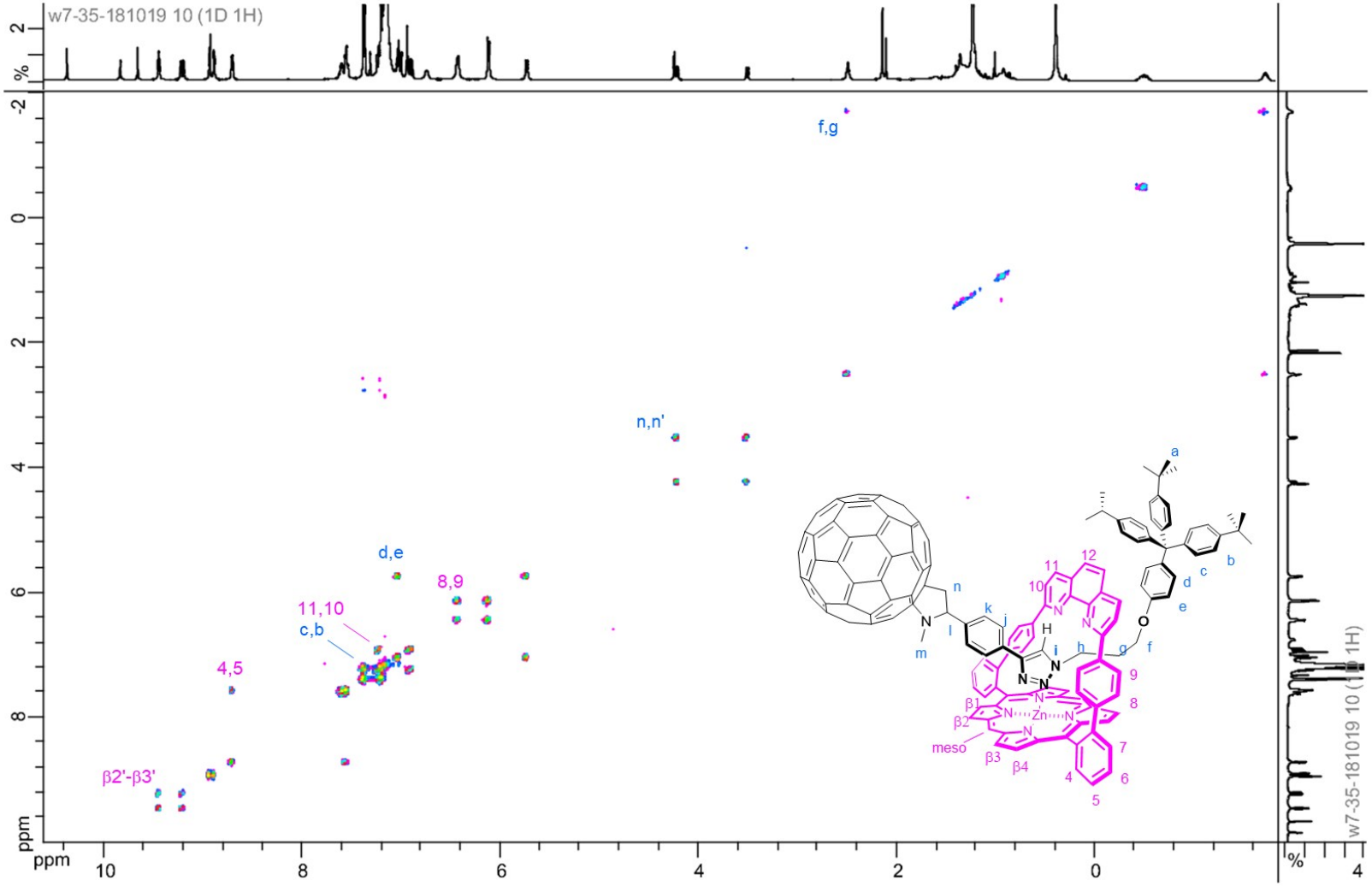

Figure S45: COSY NMR spectrum (500 MHz) of **1Zn** in benzene-d_6.

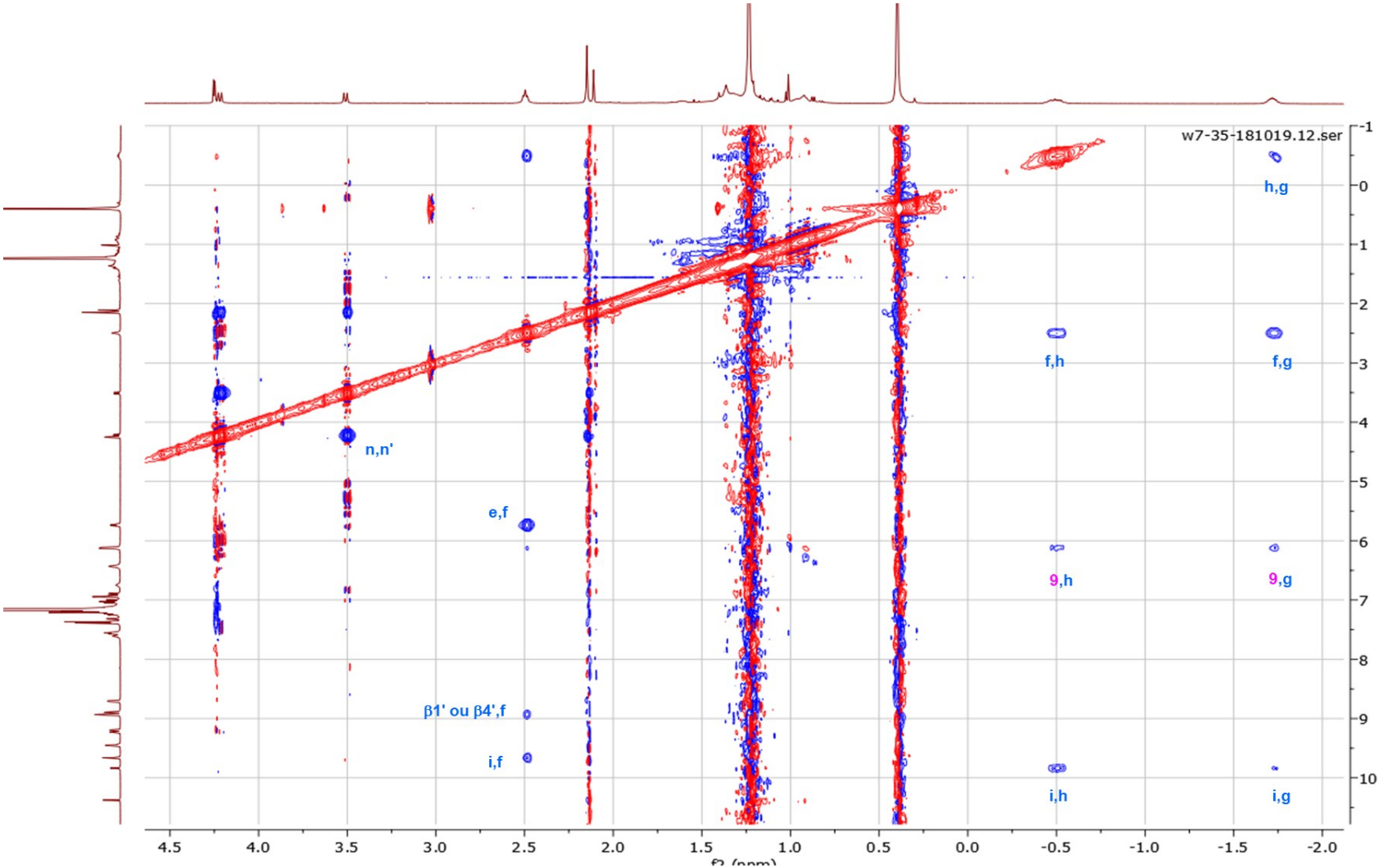

Figure S46: High field region of the ROESY NMR spectrum (500 MHz) of **1Zn** in benzene-d_6.

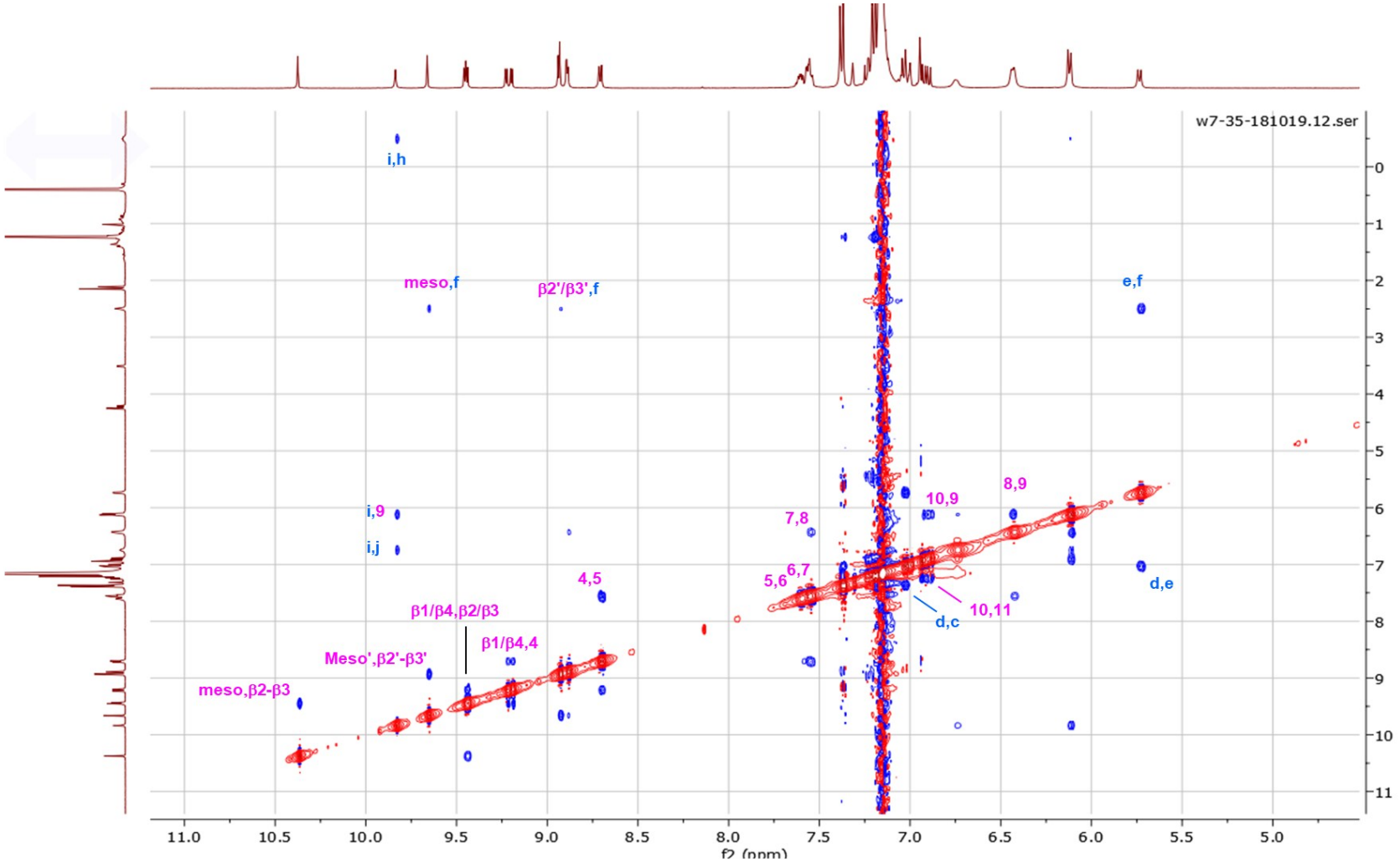

Figure S47: ROESY NMR spectrum (500 MHz) of **1Zn** in benzene-d_6 (11 ppm to 4 ppm).

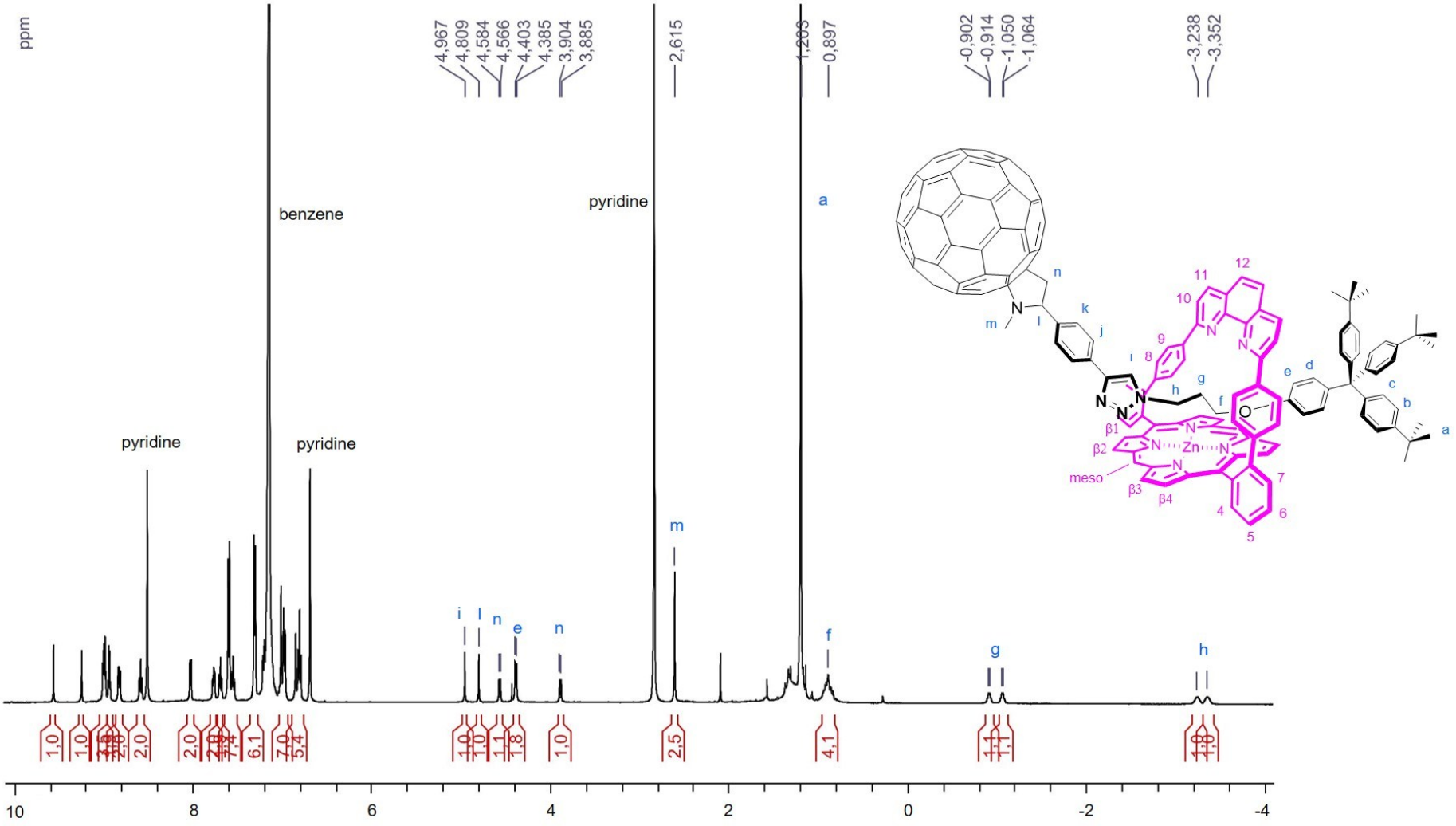

Figure S48: ^{1}H NMR spectrum (500 MHz) of **1Zn** in benzene-d_6 + 10% pyridine-d_5.

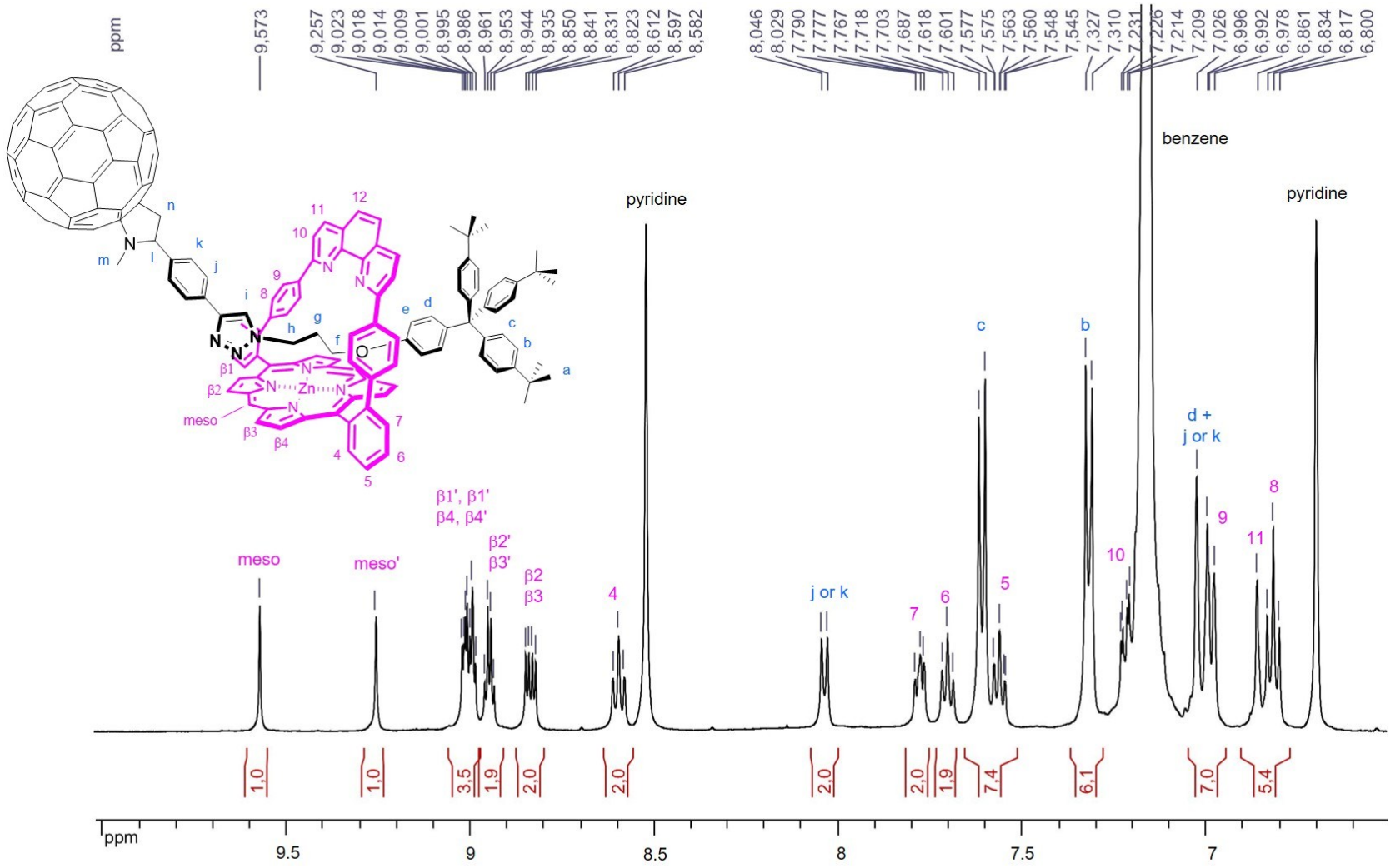

Figure S49: Aromatic region of the ^{1}H NMR spectrum (500 MHz) of **1Zn** in benzene-d_6 + 10% pyridine-d_5.

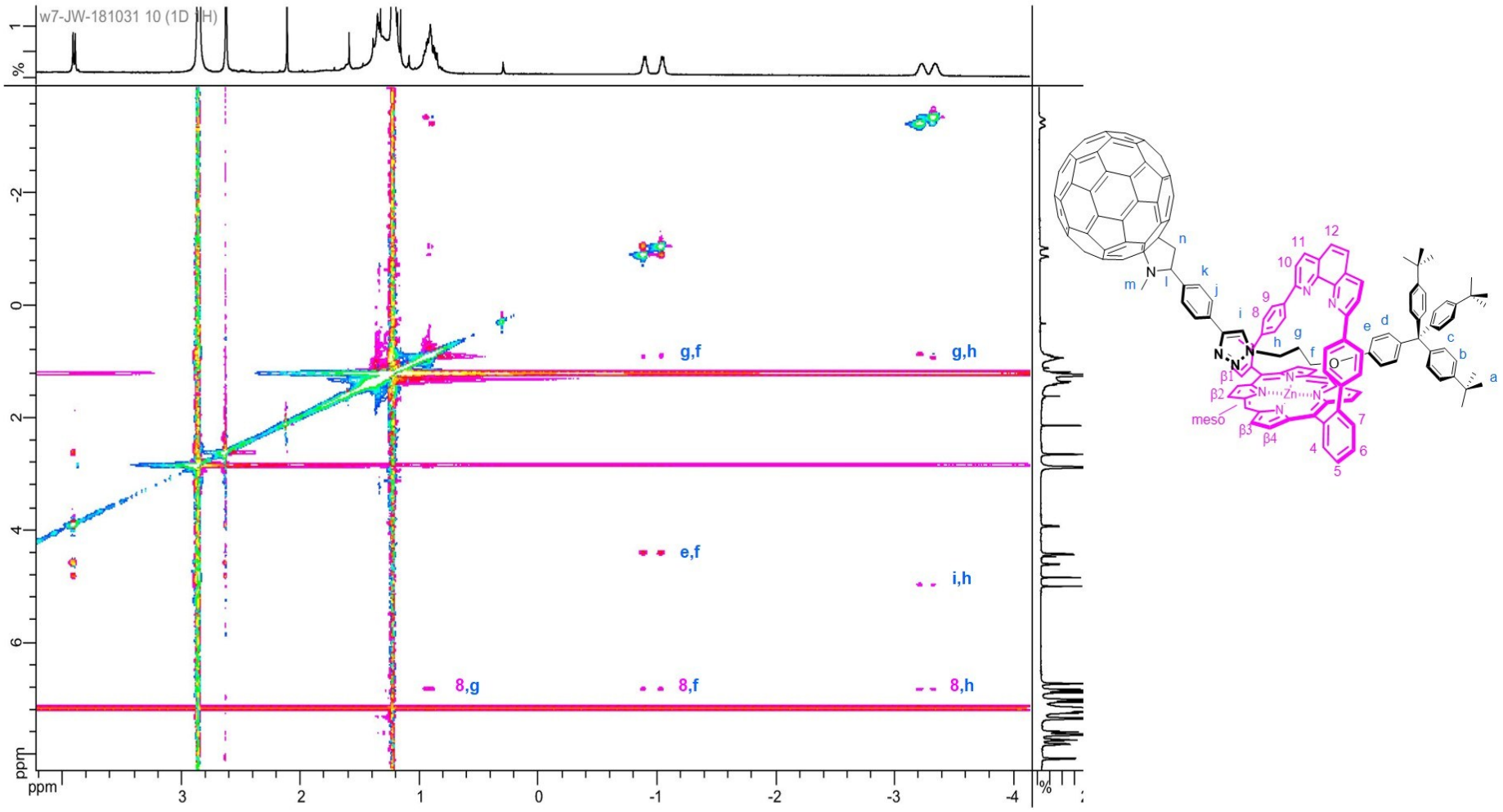

Figure S50: High field region of the ROESY NMR spectrum (500 MHz) of **1Zn** in benzene-d_6 + 10% pyridine-d_5.

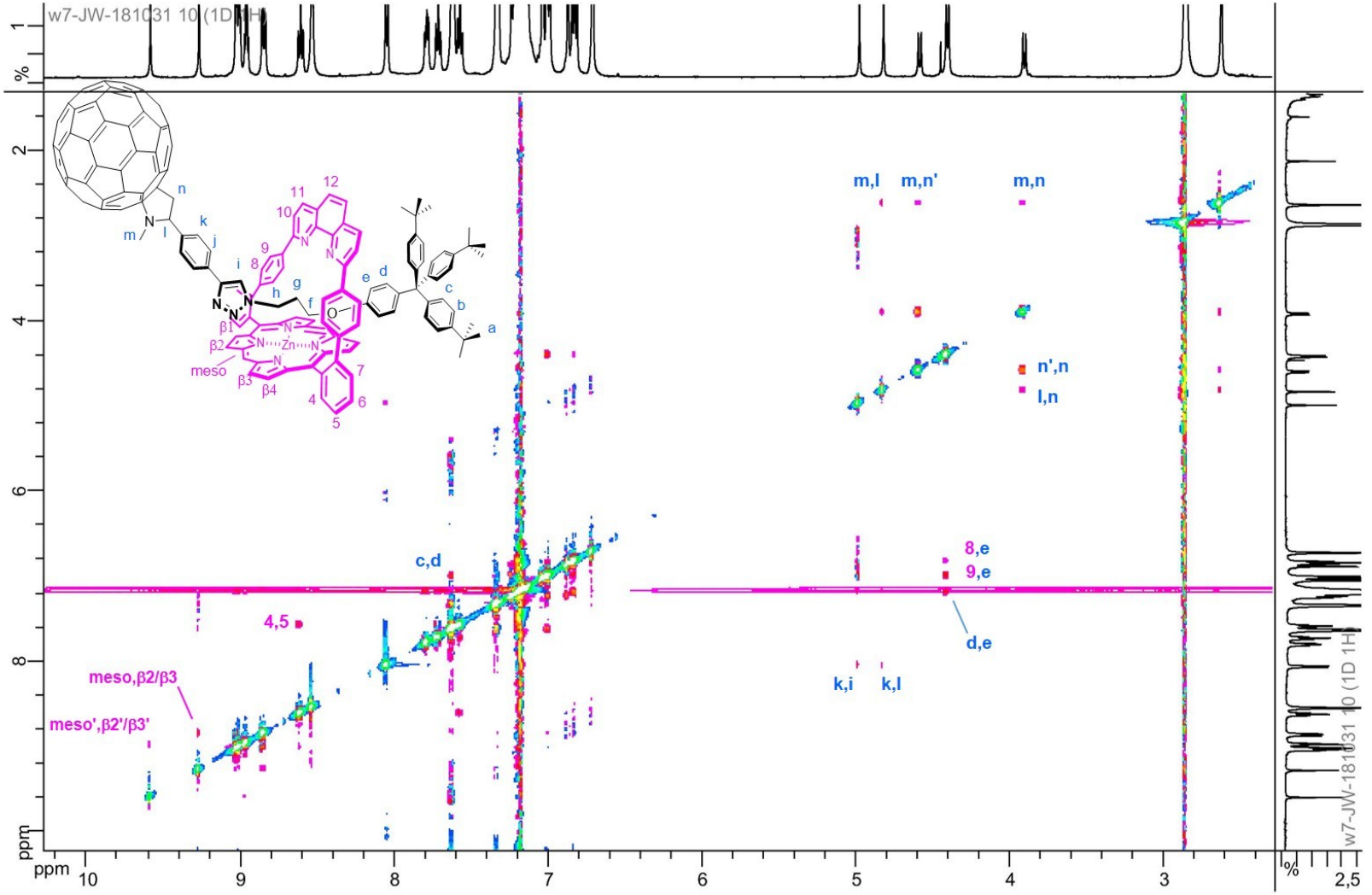

Figure S51: ROESY NMR spectrum (500 MHz) of **1Zn** in benzene-d_6 + 10% pyridine-d_5 from 10.2 to 3.5 ppm.

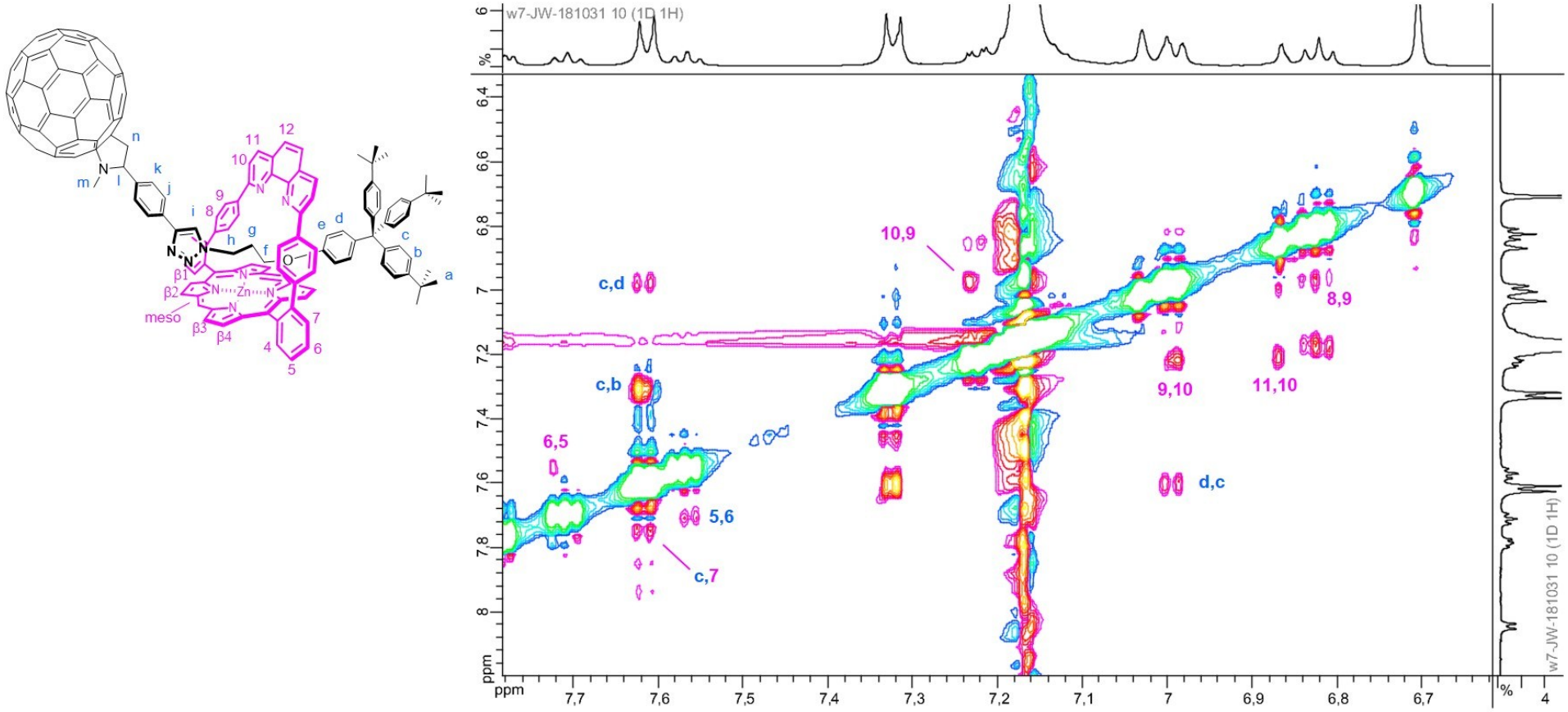

Figure S52: ROESY NMR spectrum (500 MHz) of **1Zn** in benzene-d_6 + 10% pyridine-d_5 from 7.8 to 6.6 ppm.

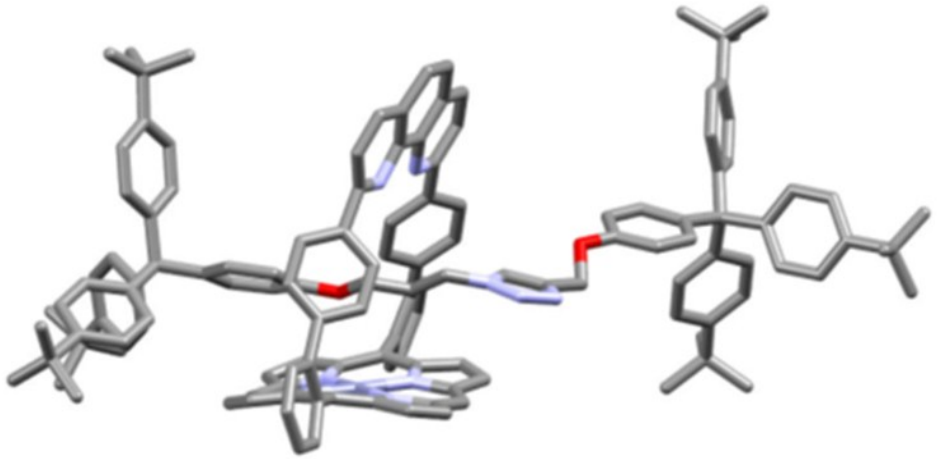

Figure S53: Crystal structure (CCDC: 1864783) of a model rotaxane showing that the triazole is not coordinated to the zinc atom of the porphyrin.